Dear Author,

Please, note that changes made to the HTML content will be added to the article before publication, but are not reflected in this PDF.

Note also that this file should not be used for submitting corrections.

AUTHOR QUERY FORM

ELSEVIER	**Journal: BBAMCR** **Article Number: 17318**	**Please e-mail or fax your responses and any corrections to:** **Person, Steve** **E-mail: Corrections.ESSD@elsevier.spitech.com** **Fax: +1 619 699 6721**

Dear Author,

Please check your proof carefully and mark all corrections at the appropriate place in the proof (e.g., by using on-screen annotation in the PDF file) or compile them in a separate list. Note: if you opt to annotate the file with software other than Adobe Reader then please also highlight the appropriate place in the PDF file. To ensure fast publication of your paper please return your corrections within 48 hours.

For correction or revision of any artwork, please consult http://www.elsevier.com/artworkinstructions.

We were unable to process your file(s) fully electronically and have proceeded by

☐ Scanning (parts of) your article ☐ Rekeying (parts of) your article ☐ Scanning the artwork

Any queries or remarks that have arisen during the processing of your manuscript are listed below and highlighted by flags in the proof. Click on the 'Q' link to go to the location in the proof.

Location in article	Query / Remark: click on the Q link to go Please insert your reply or correction at the corresponding line in the proof
Q1	Please confirm that given names and surnames have been identified correctly.
Q2, Q4, Q8	This sentence has been slightly modified for clarity. Please check that the meaning is still correct, and amend if necessary.
Q3	Journal style requires a minimum of 1 and maximum of 6 keywords. Please check and provide the necessary correction.
Q5	The given sentence seems to be incomplete. Please check for missing words/phrases and complete the sentence.
Q6, Q7, Q11, Q12	Occurrences of the citation to the "Supplement" section have been changed to "Supplementary material" for clarity. Please check and amend if necessary.
Q9	Would you consider modifying the sentence "*Determination of the spectral spillage factors S, S_1 and the α factor (in Supplement)*" to "*Determination of the spectral spillage factors S, S_1 and the α factor can be found in the Supplementary material section.*" for clarity? Please check and amend if necessary.
Q10	Occurrences of the citation to the "Supplement" section have been changed to "Supplementary materials" for clarity. Please check and amend if necessary.
Q13	Uncited references: This section comprises references that occur in the reference list but not in the body of the text. Please position each reference in the text or, alternatively, delete it. Thank you.
Q14	Please provide the corresponding grant number for the grant sponsor "European Union and the European Social Fund".

Q15	Supplementary caption was not provided. Please check suggested data if appropriate and correct if necessary. Please check this box if you have no corrections to make to the PDF file. ☐

Thank you for your assistance.

Biochimica et Biophysica Acta xxx (2014) xxx

Contents lists available at ScienceDirect

Biochimica et Biophysica Acta

journal homepage: www.elsevier.com/locate/bbamcr

Highlights

Biochimica et Biophysica Acta xxx (2014) xxx–xxx

Single-laser polarization FRET (polFRET) on the cell surface

László Bene [a,*], Tamás Ungvári [b], Roland Fedor [a], László Damjanovich [a]

[a] Department of Surgery, Medical and Health Science Center, University of Debrecen, Debrecen, Hungary
[b] Department of Biophysics and Cell Biology, University of Debrecen, Medical and Health Science Centre, Faculty of Medicine, Hungary

- Acceptor rotation measures proximity, and proximity measures donor rotation.
- Measurement of polarized fluorescence intensity components of donor and acceptor.
- Determination of the rotational characteristics and the FRET-fraction of the donors.
- Flow cytometric and rFLIM measurements on the MHCI and MHCII cell surface receptors.
- Acceptor anisotropy is more sensitive than the donor anisotropy to FRET.

http://dx.doi.org/10.1016/j.bbamcr.2014.07.011

Please cite this article as: L. Bene, et al., Single-laser polarization FRET (polFRET) on the cell surface, Biochim. Biophys. Acta (2014), http://dx.doi.org/10.1016/j.bbamcr.2014.07.011

Q15 Supplementary material.

Biochimica et Biophysica Acta xxx (2014) xxx–xxx

Contents lists available at ScienceDirect

Biochimica et Biophysica Acta

journal homepage: www.elsevier.com/locate/bbamcr

Single-laser polarization FRET (polFRET) on the cell surface

Q1 László Bene [a,*], Tamás Ungvári [b], Roland Fedor [a], László Damjanovich [a]

[a] Department of Surgery, Medical and Health Science Center, University of Debrecen, Debrecen, Hungary
[b] Department of Biophysics and Cell Biology, University of Debrecen, Medical and Health Science Centre, Faculty of Medicine, Hungary

ARTICLE INFO

Article history:
Received 21 May 2014
Received in revised form 15 July 2014
Accepted 21 July 2014
Available online xxxx

Q3 *Keywords:*
Fluorescence anisotropy
Fluorescence polarization
Fluorescence lifetime
Rotational mobility
Proximity
Receptor association
Receptor cluster
FRET-fraction
rFLIM

ABSTRACT

A new method for the simultaneous detection of rotational mobility and proximity of cell surface receptors is presented based on cell-by-cell basis measurement of polarized fluorescence intensity components of the donor and acceptor of a FRET system. In addition to the FRET efficiency and the donor and acceptor concentrations, the method makes also possible the determination of the rotational characteristics and the associated fraction of the donors (FRET-fraction). The method is illustrated with flow cytometric and rFLIM measurements on donor–acceptor systems comprising fluorescently labeled whole antibodies and their Fab fragments against Q2 epitopes of the MHCI and MHCII cell surface receptors on human lymphoblast cells. Fluorescence anisotropy of donor and acceptor and FRET efficiency were measured for samples of different acceptor-to-donor concentration ratios. Acceptor anisotropy proved to be more sensitive than the donor anisotropy for sensing FRET. After determining the rotational constants of the donor-conjugated antibodies by measurements of FRET in the steady state, and by rFLIM as a reference, the associated fractions of the MHCI and MHCII molecules in their clusters were determined. Besides the flow cytometer and the wide-field rFLIM used in this study, the method can be applied also in other devices capable of dual-anisotropy detection.

1. Introduction

Fluorescence resonance (or Förster's type of) energy transfer (FRET) is a well established sensitive tool for monitoring proximities and conformational changes of biological molecules in the 1-10 nm distance range due to the inverse sixth power distance dependence of its rate constant ($k_t \sim R^{-6}$). For the description of the phenomenon see Refs. [1–4]. Recent compilations of applications can be found in Refs. [1,5]. Several methods have been elaborated in the past for the detection of FRET in flow cytometers and microscopes by exploiting the characteristic modulation of the spectroscopic properties of the donor and acceptor fluorophores by FRET. Most of them are based on the detection of the reduction of the donor lifetime and the characteristic changes in the fluorescence intensities and the photobleaching rates of the donor and the acceptor [2].

Because FRET means a new pathway for the deactivation of the donor, the lifetime of the donor decreases [7]. In contrast, the lifetime of the acceptor remains constant because FRET at the side of acceptor means only an extra channel for excitation – sometimes also referred to as an apparent increase in acceptor lifetime – and it does not influence deexcitation. Both the reduction in the donor lifetime and the increased excitation rate of the acceptor have their consequences regarding their fluorescence emission and photobleaching rates. On the donor side, the companion phenomenon of the lifetime reduction is a decrease (or quenching) of fluorescence intensity, on the acceptor side, the companion phenomenon of the increased excitation rate is an increase in fluorescence intensity (or sensitized emission) [6,11]. As to the photobleaching rate, it behaves similarly to the fluorescence intensity: it decreases on the donor side [8–10] and increases on the acceptor side [2]. The photobleaching phenomena make possible not only the mere detection of FRET but also the direct determination of the associated fractions (or FRET-fractions) of the donors and acceptors, the associated donors and acceptors bleaching slower and faster than the not associated ones, respectively [8–10].

However, in addition to these spectral properties of the fluorophores related to their energy storing capabilities, there is another which is caused by the spatial directionality of light emission and the transversality of the photon fields freely traveling in space, namely the polarization or anisotropy of fluorescence. During FRET the anisotropy of the donor fluorescence may increase due to lifetime shortening by quenching (Fig. 1) [12–14]. Meantime the anisotropy of the acceptor fluorescence may decrease to near zero due to the excitation by a rather depolarized electric field distribution of the donor, which can be represented by a Hertzian dipole oscillator in the majority of cases [15–22]. Alternatively, the decrease may be due to a degree of randomness in

Abbreviations: FRET, fluorescence resonance energy transfer; (r)FLIM, (anisotropy-) fluorescence lifetime imaging microscopy; MHCI/MHCII, Class I/Class II Major Histocompatibility Complex protein; β_2m, beta-2 microglobulin, the light chain (l.c.) component of MHCI; mAb, monoclonal antibody; Fab, antigen binding fragment of mAb

* Corresponding author at: Department of Biophysics and Cell Biology, University of Debrecen, H-4012 Debrecen P.O. Box 39, Hungary. Tel./fax: +36 52 412 623.
E-mail address: bene@med.unideb.hu (L. Bene).

http://dx.doi.org/10.1016/j.bbamcr.2014.07.011
0167-4889/

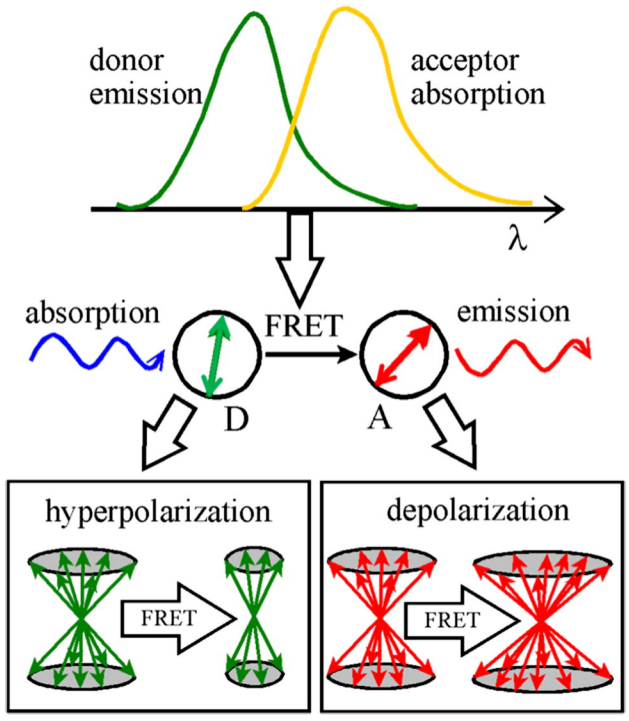

Fig. 1. Summary of the main photophysical consequences of FRET. Fluorescence intensity and anisotropy of both the donor and acceptor are affected during FRET. The acceptor takes over a portion of the energy of the donor (quenching) absorbed at a shorter wavelength and reemits a portion of it at a longer wavelength (sensitized emission) if (i) the emission spectrum of the donor and absorption spectrum of the acceptor sufficiently overlap, (ii) the interchromophore distance is in the 1–10 nm range, and (iii) the absorption moment of the acceptor is not perpendicular to the donor electric field at the location of the acceptor. While donor anisotropy increases because of the reduction of lifetime due to quenching of fluorescence, acceptor anisotropy decreases due to the depolarized way of excitation via the curvy electric field distribution of the donor dipole and the orientation randomness. The detection of these four effects – the donor quenching, acceptor sensitization, hyperpolarization of donor anisotropy, depolarization of acceptor anisotropy – can be unified in a single measuring scheme called polarization FRET (polFRET), for the simultaneous analysis of the rotational mobility and proximity of the donor–acceptor system. D: donor, A: acceptor.

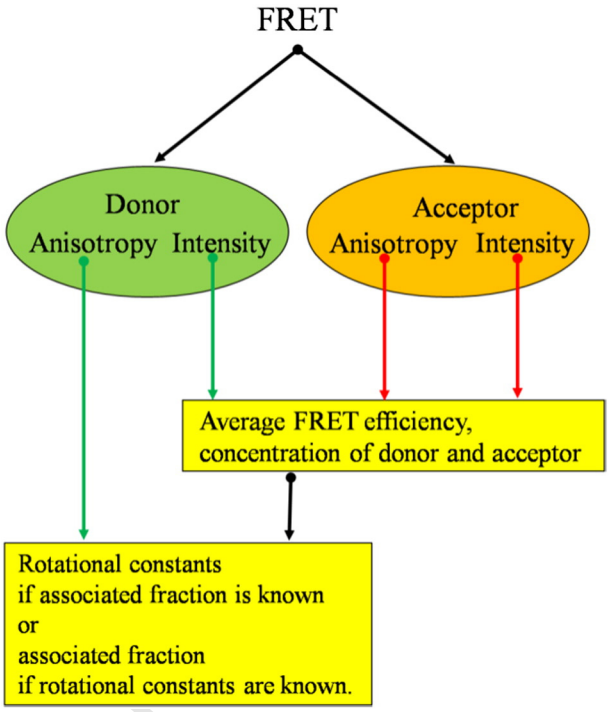

Fig. 2. The logical scheme of the polarization FRET method. The fluorescence anisotropies and intensities of the donor and acceptor are the primarily measured signals (in the ellipses). The average FRET efficiency and the amount of the donor and acceptor are those quantities computed from the acceptor anisotropy and the intensities of the donor and acceptor (in the rectangles). The donor anisotropy is used either for describing rotational motion of the donor if the associated donor fraction is known, or – as a refinement of the characterization of the receptor cluster – for the computation of the associated donor fraction if the rotational constants of the donor are known.

the orientation distribution of acceptor relative to the donor's, manifested in characteristic values of the κ^2 orientation factor (2/3 and 0.475 hold for the dynamic and the static averaging regimes, respectively) [4,18–20,22].

Steady state methods of FRET determination based on the Perrin-equation have been elaborated earlier based on the detection of enhancement of donor-anisotropy upon lifetime shortening (QREA, quenching resolved emission anisotropy) [12,14]. Furthermore, the relationship between the donor anisotropy and FRET were investigated by frequency domain lifetime fluorometry [23]. The only possibility for the detection of homo-energy transfer (FRET between identical fluorophores, also called energy-migration FRET) having small Stokes' shift is essentially based on the reduced anisotropy of the sensitized emission, since the fluorescence emissions of the directly and indirectly excited fluorophores are indistinguishable. These two methods can also be called "dynamic" and "static" anisotropy measurements, because in the "dynamic" case the presence of some rotational mobility of the donor ("transfer rotational modes") enhances FRET sensitivity and in the "static" case the absence of these modes improves the ability to detect FRET [14,21,24].

Our work was motivated by two purposes (see a flow-chart summary in Fig. 2): (i) Exploitation of the extra degrees of freedom offered by the donor and acceptor anisotropies for the extension and completion of the single laser FRET detection method published earlier by Szöllősi et al. [24]. (ii) The application of the new method for the resolution of association heterogeneity of cell surface receptors i.e. to determine the associated fraction of the donors (also called FRET-fraction).

In the first approach (if the possible association heterogeneity is neglected) the FRET problem poses three unknowns i.e. it has three degrees of freedom: the FRET efficiency and the amount of the donor and acceptor as represented by the would-be hypothetical intensities of the donor and acceptor when FRET is "switched off". Accordingly, the full description of the system requires the detection of three independent signals [6,11]. In the conventional single laser excitation method only two signals, the donor and acceptor intensities excited around the absorption maximum of the donor are detected making possible the determination of only two unknowns. The missing third signal is replaced by an assumption on the acceptor-to-donor concentration (intensity) ratio, namely that its value on the double labeled sample is the same as that estimated from the intensities of the single-labeled samples. Although, notwithstanding the above simplification, the method is generally superior than those based on the detection of the donor or acceptor intensities alone, in the case of spatially interacting dye targeting ligands (e.g. competition or allosteric modulation during binding of the donor- and acceptor-conjugated ligands) the assumption of the interaction free value of the acceptor-to-donor ratio can lead to significant systematic errors in the FRET efficiency. However, this shortcoming of the method can be overcome by the detection of a third independent signal in addition to the donor and acceptor intensities at the donor's excitation wavelength. This signal can be e.g. a third fluorescence intensity at the excitation wavelength of the acceptor as in the dual laser flow cytometric FRET (also called FCET) method elaborated earlier in our laboratories [6,11].

Alternatively, the two polarized components of the acceptor intensity, i.e. the total intensity and the anisotropy of the acceptor at the donor's excitation wavelength can also be detected. At this stage, another hurdle arises due to the possible intensity (and anisotropy) cross-talks of the

Please cite this article as: L. Bene, et al., Single-laser polarization FRET (polFRET) on the cell surface, Biochim. Biophys. Acta (2014), http://dx.doi.org/10.1016/j.bbamcr.2014.07.011

donor and acceptor, a nuisance accompanying the necessary spectral overlap of the donor and acceptor emissions. The spectral unmixing of fluorescence intensities and anisotropies necessitates the detection of the polarized intensity components also for the donor emission.

However, by the simultaneous detection of the four polarized intensity components our problem becomes over determined, i.e. we have four independent parameters making possible the determination of an additional fourth unknown. This unknown can be the rotational characteristics of the donor in the case of homogeneous donor association (unity FRET-fraction) or as a refinement of our cluster determination, the degree of association heterogeneity (the FRET-fraction) if the rotational characteristics of the donor are known (see also Fig. 2). The reasoning behind this kind of an approach is the fact that when only a portion of the donors is associated with acceptors both the detected donor anisotropy and the energy transfer efficiency are averages on the clustered and unclustered donor fractions. The simultaneous measurement of these quantities makes possible the assessment of both the clustered donor fraction and the true energy transfer efficiency characterizing the clustered fraction (anisotropy resolved FRET and FRET-fraction). As a summary of this section, since fluorescence anisotropy of the donor is altered by FRET in a characteristic fashion it can be used as a new contrast parameter either for the resolution of FRET heterogeneities due to e.g. partial association of receptors if the rotational motion of the donor is clarified, or for the resolution of the contributions of changes in distance and orientation (or rotational mobility) during a conformational transition, if the associated fraction of the donors is known.

The new and the conventional versions of the single-laser method are compared in the measurements of homo- and heteroassociations of the MHCI and MHCII receptors on the surface of Kit-225-K6 T-cells and JY B-lymphoblast cells, two cell lines the receptor clusters of which have already been characterized in detail with different methods in our laboratory [26–32]. These receptors, which are fairly abundant on these cells (1–2 millions/cell), form intensive homo- and heteroassociations, with their roles in mediating immune recognition by the helper and killer T-cells via avidity modulation, in maintenance of the signal-transduction platforms called lipid rafts, and also in active signaling toggling between apoptosis and activation. Donor- and acceptor-conjugated mAbs or their Fab fragments to the light and heavy chains of the MHCI (L368 and W6/32 mAbs, respectively) and to the MHCII receptor (L243 mAb) have been used as the illustrating FRET-systems.

The buildup of the material is the following: First the new and the conventional methods are compared in flow cytometric and rFLIM measurements using sterically non-interacting and interacting mAbs. Besides that the intramolecular FRET between the fluorescently stained L368 mAb against the β_2-microglobulin and the W6/32 mAb against the heavy chain of the MHCI molecule serves as positive control for a high level of FRET, these mAbs are not interacting. The non-interacting case is important because based on the conventional method which is expected to be applicable in this case, the anisotropy of sensitized emission can be measured, and the validity of our assumption on its zero value can be checked. In the interacting cases of the MHCI homoassociation and the MHCII–MHCI heteroassociation systematic differences can be expected between the two methods due to the significant competition between the involved mAbs (L243 against MHCII, and L368 or W6/32 against MHCI). Because the resolution of the method is expected to depend on – amongst many other factors – the starting anisotropies of the single donor and acceptor labeled samples, test measurements were carried out with both whole mAbs and their Fab fragments in samples where FRET was changed by titration of the amount of acceptor mAbs.

After comparing the two methods, rFLIM and flow cytometric analyses of rotational parameters of the donor-conjugated L368, W6/32 and L243 whole mAbs and their Fabs are presented. In the case of the L368 and W6/32, two not-competing mAbs binding to the β_2-microglobulin and heavy chain components of the same MHCI molecule with a 1:1 stoichiometry, the rotational parameters were also determined with flow cytometric recording of FRET-resolved Perrin-plots, based on the fact that the associated fraction in this case is determined by the stoichiometry of labeling i.e. the acceptor-to-donor ratio which can be adjusted at custom. The rotational constants– the r_0 limiting anisotropy and the ϕ rotational correlation time – are used later for determining the associated fractions in the MHCI homoassociations and MHCII–MHCI heteroassociations.

Error propagation and detection sensitivity are detailed quantitatively in the Supplementary material.

2. Materials and methods

2.1. Cell lines

The Kit-225-K6 cell line is a human T cell with helper phenotype and with an IL-2 requirement for its growth [33]. The JY B cell line was originally described in [34]. Both cell types were cultured in RPMI-1640 medium supplemented with 10% fetal calf serum, penicillin and streptomycin [34]. To the Kit-225-K6 cells 20 U/ml recombinant interleukin-2 (IL-2) was also added every 48 h.

2.2. Monoclonal antibodies

The production and specificity of monoclonal antibodies (mAbs) applied in the experimental procedures have been described earlier [28,35]. MAbs W6/32 (IgG_{2a6}) and L368 (IgG_{16}) developed against a monomorphic epitope on the α_2, α_3 domains of the heavy chain and the β_2-microglobulin of MHCI, respectively [28,35,36]; mAb L243 (IgG_{2a6}) against MHCII, DRV were kindly provided by Dr. Frances Brodsky (UCSF, CA). These mAbs were prepared from supernatants of hybridomas and were purified by affinity chromatography on protein A-Sepharose.

2.3. Preparation of Fab fragments

Fab fragments of the purified antibodies were prepared by papain digestion at an antibody/enzyme (w/w) ratio of 100, at 37 °C for 4–12 h [37,38]. The digestion products were subjected to ion-exchange chromatography on DEAE-Sephacel (Pharmacia). The Fab fragments eluted in the flow-through fraction were freed of undigested IgG and of the Fc fragments. Control of the digestion and Fab purification was carried out by SDS/PAGE, enzyme immunoassay, and size-exclusion chromatography on Sephacryl S-100 or analytical ultracentrifugation (Beckman Model E).

2.4. Fluorescent staining of antibodies

Aliquots of the proteins for fluorescence were labeled with Alexa-Fluor 488 (AF488) as the donor dye and Alexa-Fluor 546 (AF546) as the acceptor dye (Invitrogen). Kits provided with the dyes were used for the conjugation. Detailed labeling procedure of the mAb was described earlier [28,39,40]. Dye-per-protein labeling ratios (L) for the donor-conjugated L243, L368, and W6/32 whole mAbs were 2.3 (or 1.86), 2.11 (or 4.96), and 2.69, respectively; for their Fab fragments they were 0.84 (or 0.95), 1.57, and 0.89, respectively. The labeling ratios for the acceptor-conjugated L243, L368, and W6/32 whole mAbs were 2.72, 3.11 (or 1.68), and 2.1 (or 3.46), respectively; for their Fab fragments they were 1.42, 1.34, and 0.89, respectively. These values were separately determined for each labeled aliquot in a spectrophotometer (Shimadzu UV-2100) [28]. Fluorescently labeled antibodies retained their biological activity according to competition with unlabeled proteins in binding to membranes of living cells.

Please cite this article as: L. Bene, et al., Single-laser polarization FRET (polFRET) on the cell surface, Biochim. Biophys. Acta (2014), http://dx.doi.org/10.1016/j.bbamcr.2014.07.011

2.5. Labeling of cells with mAbs

Freshly harvested cells were washed twice in ice cold PBS (pH 7.4), the cell pellet was suspended in 100 μl of PBS (10^6 cells/ml) and labeled by incubation with ~10 μg of dye-conjugated mAbs for 40 min on ice in the dark. The excess of mAbs was at least 30-fold above the K_d during incubation. To avoid possible aggregation of the dye-conjugated mAbs, they were air-fuged (at 110,000 *g*, for 30 min) before labeling. Special care was taken to keep the cells at ice cold temperature before FRET measurements in order to avoid unwanted aggregations of cell surface receptors or receptor internalization. Labeled cells were washed twice with ice cold PBS and then fixed with 1% paraformaldehyde.

The single acceptor-labeled and the double-labeled (with both donor and acceptor) samples were titrated according to the surface concentration of the acceptor carrying mAb. In these samples the cells were treated identically, except for the amount of acceptor-stained antibodies used for labeling: it has been gradually increased until the final saturating concentration was achieved. The final concentrations in the titration series in μM for the whole mAbs L243, L368, and W6/32 were 0.677, 0.734, and 0.686, respectively; for the Fab fragments of L243, L368, and W6/32 they were 0.768, 0.754, and 0.779, respectively.

2.6. Determination of expression level of receptors

The relative expression levels of receptors on Kit-225-K6 cells were: MHCI, 100 ± 13.3%; MHCII, 73.8 ± 1.2%, where the 100% level means an absolute copy number of (1–1.5) × 10^6. On JY cells: MHCI, 100 ± 13.3%; MHCII, 60.9 ± 9.7%, where the 100% level means an absolute copy number of (1.5-2) × 10^6. The number of binding sites was determined from the mean values of flow-cytometric fluorescence intensity histograms of cells labeled to saturation with dye-conjugated mAbs (Scatchard-analysis). The mean fluorescence intensities were converted to the number of binding sites by calibration with fluorescent microbeads having known number of fluorescent dyes (Rainbow Fluorescent Particles, 3.0–3.4 μm in diameter, Catalog Number: 556291, BD Biosciences, Pharmingen). They were also used for the calibration of the forward angle light scattering (FSC) signals in the determination of cell size: 13–14 μm and 20–25 μm for the Kit-225-K6 and JY cells, respectively.

2.7. Flow cytometric dual-anisotropy measurements

Cell-by-cell basis correlated measurements of the polarized intensity components – i.e. the total intensities and anisotropies – of the donor and acceptor were carried out in a "dual T-format" arrangement [41,42]. It was realized in a modified FACStar^{Plus} flow cytometer (Becton Dickinson, CA) by placing two polarization beam splitter cubes (broadband polarization beamsplitter cube, model 10FC16PB.3, Newport) in the donor and acceptor fluorescence channels (Fig. 3). The fluorescence intensities of the green (Alexa-Fluor 488) donor dye and the red acceptor dye (Alexa-Fluor 546) were excited at the 514-nm line of an Argon-ion laser (Model Stabilite-2017, Spectra Physics, Mountain View, California) and were detected orthogonally to the direction of the exciting laser light beam by green and red sensitive photomultiplier tubes (Hamamatsu). After transmitting through a 525-nm long path filter to reduce background due to the light scattering (HQ525 lp, all HQ filters used were manufactured by AF Analysentechnik, Tübingen) the donor and acceptor fluorescence intensities were partially separated by a suitable dichroic mirror (DM in Fig. 3, manufactured by Ferenc Kárpát, Central Physics Research Institute, Budapest, Hungary), and subsequently detected either at 535 ± 15 nm (fluorescence channel of the donor, channel 1) or at 640 ± 60 nm (fluorescence channel of the acceptor, channel 2) (filters HQ535/30 bp and HQ 640/120 bp). The donor and acceptor fluorescence intensities were further split by the broadband polarization beam splitter cubes (10FC16PB.3, Newport) into their vertical and horizontal components before reaching the respective photomultipliers. For the determination of the G-factor of each fluorescence channel, the vertical polarization direction of laser light was rotated by 90° with a Fresnel-type double-rhomb polarization rotator (broadband polarization rotator, model PR-550, Newport).

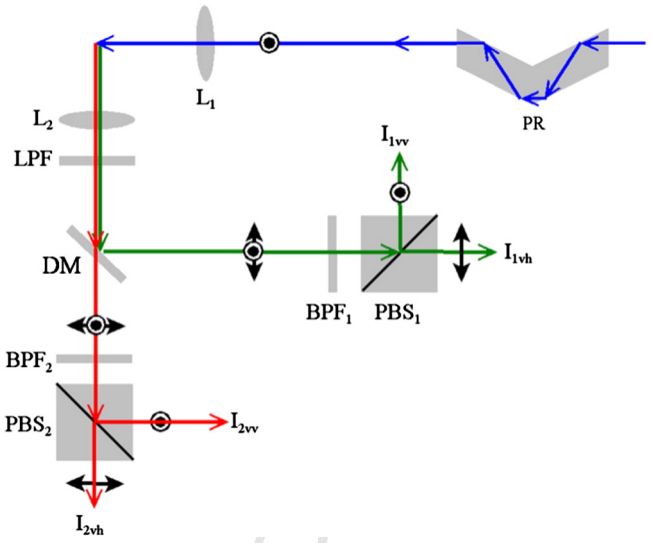

Fig. 3. Scheme of the "dual T-format" optical arrangement for the unified measurement of the donor and acceptor anisotropies: single laser polarization energy transfer (polFRET). The cells are illuminated through an L_1 focusing lens, the fluorescence of the donor (green) and acceptor (red) is collected by a lens L_2 (NA = 0.6) and lead through the long path filter LPF (525 nm) to cut off reflected and scattered laser light (blue). After separation by the DM (550 nm LP) dichroic mirror beam splitter and a further spectral cleaning by the BPF_1 (535 ± 15 nm) and BPF_2 (640 ± 60 nm) band path filters, the donor and acceptor intensities are split by the polarization beam splitters PBS_1 and PBS_2 into parallel and horizontal components. The polarization direction of the illuminating laser light can be rotated into the perpendicular direction for the measurement of the G-factors by the PR polarization rotator ("double Fresnel-rhomb"). The polarization direction in the plane of the drawing (horizontal) is represented by double-ended arrows, the perpendicular polarization (vertical) by encircled dots.

Four polarized intensities have been detected for each fluorescence channel: I_{ivv}, I_{ivh}, I_{ihv}, and I_{ihh}, with the first index *i* designating the signal channel, the second and third ones referring to the polarization direction of the exciting laser light and that of the fluorescence, respectively. After subtracting the corresponding background intensities measured on the unlabeled cells from the polarized intensities, the correction factors G_i (i = 1, 2) balancing the sensitivities of vertical and horizontal fluorescence channels, the total fluorescence intensities I_i, and the fluorescence anisotropies r_i were calculated as follows:

$$G_i = I_{ihv}/I_{ihh}, \quad (1)$$

$$I_i = I_{ivv} + a(\psi) \times G_i \times I_{ivh}, \quad (2)$$

$$r_i = (I_{ivv} - G_i \times I_{ivh})/I_i. \quad (3)$$

In the above expression for the total intensities I_i (i = 1,2) a numerical correction for the high aperture fluorescence collection was carried out according to T.M. Jovin [21,43] by using the term $a(\psi) = 1 + \cos\psi \cdot (1 + \cos\psi)/2$, where $a(\psi)$ assumes a value of 1.72 for our numerical aperture of NA = 0.6, and ψ stands for the half angle of the detected light cone. The anisotropy and total intensity values were computed on a cell-by-cell basis from the correlated I_{ivv} and I_{ivh} intensities with predetermined values of the G_i factors as input parameters. Based on Eq. (2) the r_{corr} aperture-corrected anisotropy can be written as the function of the r uncorrected one as follows: $r_{corr} = 3 \cdot r/\{1 + a(\psi) + r \cdot [2 - a(\psi)]\}$.

Please cite this article as: L. Bene, et al., Single-laser polarization FRET (polFRET) on the cell surface, Biochim. Biophys. Acta (2014), http://dx.doi.org/10.1016/j.bbamcr.2014.07.011

The mean values of fluorescence anisotropy and total intensity histograms measured on the single donor- or acceptor-labeled cells (~10^4) were further used for the calculation of the necessary input constants α, S_1, $f_{a/d}$, r_a for constructing the histograms of different quantities determined from the double-labeled energy transfer samples such as the set of quantities E, r_{et}, I_d, I_a (Eqs. (17)–(21)) or the set of T, I_d, I_a (Eqs. (31)–(34)). The average values of the means of anisotropy histograms obtained in different measurements with their standard errors were also determined and are listed in Tables 1, 3. The generation and subsequent analysis of flow cytometric histograms (see also Fig. 4 for examples) and 2-dimensional correlation plots (dot-plots) of total fluorescence intensities, fluorescence anisotropy, and energy transfer efficiency were performed by a home-made software specialized for flow cytometric data analyses called Reflex, written by G. Szentesi [44], freely downloadable from http://www.biophys.dote.hu/research.htm, and http://www.freewebs.com/cytoflex.htm.

Reference measurements by fluorescence anisotropy-lifetime imaging microscopy (rFLIM), are found in the Supplementary material.

3. Theoretical results

3.1. Theory of polFRET

3.1.1. Spectral unmixing of the measured intensities and anisotropies

In this method of FRET determination both the donor and acceptor are simultaneously excited at a suitable illumination wavelength and the polarized components of the fluorescence intensities are measured in a "dual T-format" configuration [41,42] (Fig. 3). Generally, due to the broadness and small wavelength separation of the emission spectra of the fluorophores the measured total intensity and anisotropy signals should be corrected for the spectral overlaps (or spillages) to obtain the pure donor and acceptor signals. In the following section the way of spectral correction of the total intensities and fluorescence anisotropies of the double-labeled sample as computed according to Eqs. (1)–(3) is summarized.

According to Eq. (4), the I_1 total fluorescence intensity measured in the donor channel can be decomposed into the sum of the 1st term corresponding to the donor intensity reduced by FRET; the 2nd term, a portion (or cross-talk) of the directly excited acceptor fluorescence; and the 3rd term, a portion (or cross-talk) of the acceptor fluorescence excited indirectly by FRET (or sensitized emission) [6,11,25]:

$$I_1 = I_d \cdot (1-E) + I_a \cdot S + I_d \cdot E \cdot \alpha \cdot S. \quad (4)$$

Here E is the FRET efficiency. The S is a spillage factor expressing the overlap of the acceptor emission with the donor channel, and the factor α takes into account the different sensitivity of the donor and acceptor channels in detecting a single green and red photon (see the Supplementary material for their details) [49]. The quantities I_d and I_a, which cannot be measured directly, are the hypothesized "would be" donor and acceptor fluorescence intensities unperturbed by FRET and with E, they constitute the 3 unknowns of the FRET problem. They are proportional to the actual amount of the donor and acceptor on the double-labeled cells. The fluorescence intensity I_2 detected in the acceptor channel can be decomposed into donor and acceptor contributions in a similar way, described by the 1st term, cross-talk of the remaining donor intensity; 2nd term, directly excited acceptor emission; and the 3rd term, the sensitized emission i.e. a portion of the donor's missing energy reradiated by the acceptor:

$$I_2 = I_d \cdot (1-E) \cdot S_1 + I_a + I_d \cdot E \cdot \alpha \quad (5)$$

where S_1 designates the spillage factor expressing overlap of the donor emission with the acceptor channel (see next section about its details).

Table 1
Input parameters for the computation of the conventional (E) and polarization FRET efficiencies (T) — a case study on Kit-225-K6 T-lymphoma cells.

Donor (AF488-conjugated)		Acceptor (AF546-conjugated)		Single-labeled samples								Double-labeled samples							
mAb	Antigen	mAb[a]	Antigen	L_d[a]	L_a[a]	r	ρ_d	S_1[b]	r_a	$(B_a/B_d)_0$	α[b]	r_1	r_2	S_1'[b]	r_a'	E (%)	r_{et}	T (%)	B_a/B_d
Part A, whole mAbs																			
L368	β_2m	W6/32(1)[a]	MHCI h.c.	2.11	2.10	0.216	0.887	0.308	0.287	0.273	0.97	0.222	0.181	1.140	0.175	21.9[c]	−0.056	25.1[c]	0.237
		W6/32(2)							0.274	0.381		0.226	0.177	1.661	0.171	31.9	−0.032	34.4	0.346
		W6/32(3)							0.222	0.771		0.235	0.179	2.821	0.175	36.6	0.013	35.3	0.801
		W6/32(4)							0.221	0.938		0.243	0.169	3.753	0.165	44.0	−0.031	47.3	0.848
		W6/32(5)							0.221	0.995		0.243	0.167	4.945	0.164	54.2	−0.009	55.2	0.962
Part B, whole mAbs																			
W6/32	MHCI h.c.	W6/32(1)	MHCI h.c.	2.69	2.10	0.190	0.911	0.319	0.287	0.226	0.97	0.197	0.152	0.855	0.135	20.7	−0.127	22.6	0.156
		W6/32(2)							0.274	0.239		0.202	0.152	0.962	0.136	23.6	−0.063	25.0	0.191
		W6/32(3)							0.222	0.535		0.215	0.152	1.640	0.141	28.4	−0.057	33.2	0.447
		W6/32(4)							0.221	0.652		0.219	0.158	2.281	0.151	39.1	0.001	39.0	0.655
		W6/32(5)							0.221	0.690		0.222	0.157	2.910	0.151	48.5	0.024	45.6	0.772
Part C, Fab fragments																			
L368 Fab	β_2m	W6/32Fab(1)	MHCI h.c.	1.57	0.89	0.230	0.957	0.112	0.320	0.306	0.63	0.237	0.174	0.527	0.161	22.4	−0.042	24.6	0.266
		W6/32Fab(2)							0.288	0.429		0.238	0.174	0.678	0.163	26.1	−0.030	28.1	0.390
		W6/32Fab(3)							0.256	0.788		0.250	0.180	1.426	0.175	43.6	0.037	39.9	0.912
		W6/32Fab(4)							0.260	0.923		0.253	0.173	1.495	0.168	41.6	−0.024	43.8	0.849
		W6/32Fab(5)							0.225	0.963		0.248	0.171	1.783	0.167	47.9	0.059	40.4	1.253
Part D, Fab fragments																			
W6/32 Fab	MHCI h.c.	W6/32Fab(1)	MHCI h.c.	0.89	0.89	0.210	0.890	0.121	0.320	0.095	0.63	0.226	0.147	0.341	0.117	17.0	−0.107	18.1	0.063
		W6/32Fab(2)							0.288	0.130		0.229	0.151	0.432	0.129	20.2	−0.053	21.4	0.105
		W6/32Fab(3)							0.256	0.239		0.239	0.156	0.701	0.144	22.1	0.007	21.7	0.224
		W6/32Fab(4)							0.260	0.255		0.255	0.164	1.451	0.161	54.3	0.084	25.5	0.436
		W6/32Fab(5)							0.225	0.265		0.251	0.163	1.245	0.156	48.3	0.094	26.5	0.486

[a] L designates the dye-per-protein labeling ratio (D/P). The numbers in parenthesis indicate acceptor concentrations in increasing order, as specified in Section 2.

[b] Because parameters S_1, α, and S_1' depend on the optical alignment of the flow cytometer, they can be subjected to day-to-day variations even for a given donor–acceptor pair. All values are averages for three different samples run under the same optical alignment. The relative errors for the means (CVs), which are not indicated for clarity, are under 10%.

[c] FRET efficiencies computed without and with fluorescence anisotropy are designated by E and T, respectively. Determination of E is based on acceptor-to-donor receptor number ratios $(B_a/B_d)_0$ obtained from single-labeled samples. Acceptor-to-donor receptor number ratios determined from single- and double-labeled samples are designated by $(B_a/B_d)_0$ and B_a/B_d, respectively.

Please cite this article as: L. Bene, et al., Single-laser polarization FRET (polFRET) on the cell surface, Biochim. Biophys. Acta (2014), http://dx.doi.org/10.1016/j.bbamcr.2014.07.011

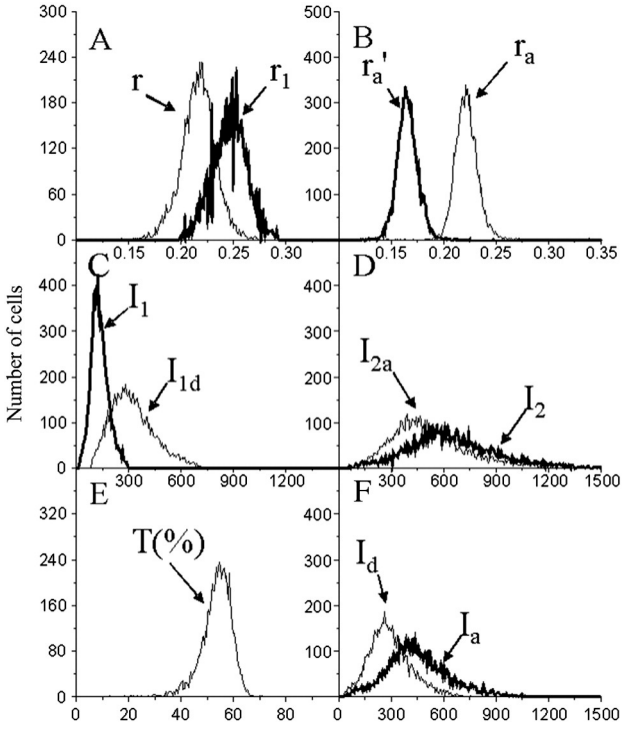

Fig. 4. The collection of the primary frequency distribution curves of the polFRET method. Shown are flow cytometric frequency distribution curves of the primarily measured anisotropy (r, r_1, r_a, r_a') and intensity (I_1, I_{1d}, I_2, I_{2a}) signals, the deduced FRET efficiency (T) and the donor and acceptor intensities (I_d, I_a) unperturbed by FRET for the β_2m-MHCI h.c. system on the Kit-225-K6 human T-lymphoblast cells. Panel A: hyperpolarization of donor anisotropy; r, single donor-labeled sample, r_1, double-labeled (transfer) sample. Panel B: depolarization of acceptor anisotropy; r_a, single acceptor-labeled sample, r_a' double-labeled sample, after demixing the spectral cross-talk of the donor. From Panels A and B it can be seen that the acceptor anisotropy is more affected than the donor anisotropy by the same magnitude of FRET. Panel C: quenching of donor fluorescence; I_{1d}, single donor-labeled sample, I_1, double-labeled sample. Panel D: sensitization of acceptor fluorescence; I_{2a}, single acceptor-labeled sample, I_2, double-labeled sample. Panel E: computed FRET efficiency T. Panel F: computed intensities I_d and I_a, signals proportional to the donor and acceptor concentration, respectively in the double labeled sample when FRET is "switched off". d: donor (Alexa-Fluor 488 targeted by the L368 mAb), a: acceptor (Alexa-Fluor 546, targeted by the W6/32 mAb), t: donor- and acceptor-labeled (FRET) sample. Note that while the width of donor-anisotropy distribution curve increases (Panel A) implying decreased signal-to-noise ratio due to donor quenching, the width of the acceptor-anisotropy distribution curve decreases (Panel B) implying increased signal-to-noise ratio due to acceptor sensitization.

Based on the additivity law of fluorescence anisotropy [41,42], the r_1 and r_2 net anisotropies detected in the donor and acceptor channels can be written as averages of the donor anisotropy r' and acceptor anisotropies r_a and r_{et} with the corresponding intensity terms of Eqs. (4) and (5) as weighting factors:

$$r_1 = \left[I_d \cdot (1-E) \cdot r' + I_a \cdot S \cdot \rho_a \cdot r_a + I_d \cdot E \cdot \alpha \cdot S \cdot \rho_a \cdot r_{et}\right]/I_1, \quad (6)$$

$$r_2 = \left[I_d \cdot (1-E) \cdot S_1 \cdot \rho_d \cdot r' + I_a \cdot r_a + I_d \cdot E \cdot \alpha \cdot r_{et}\right]/I_2, \quad (7)$$

where r' designates the FRET-enhanced fluorescence anisotropy of the donor, and r_a and r_{et} the anisotropies of acceptor fluorescence excited directly or indirectly by FRET, respectively. The correction factors ρ_d and ρ_a defined as

$$\rho_d = (r_2/r_1)_{\text{donor only}} \quad (8)$$

and

$$\rho_a = (r_1/r_2)_{\text{acceptor only}} \quad (9)$$

take into account possible dependence of the anisotropies on the emission wavelength and/or the optics of the detection channels, and they can be determined using cells labeled with only donor or acceptor. The factor ρ_d might also be connected to the difference in lifetime heterogeneities of the two signal channels (see also Section 5). By the introduction of the quantity r_a', the total anisotropy of acceptor in the presence of the donor is actually an average of the r_a directly excited transfer-free anisotropy and the r_{et} anisotropy of the sensitized emission with the corresponding intensities as weighting factors:

$$r_a' = (I_a \cdot r_a + I_d \cdot E \cdot \alpha \cdot r_{et})/(I_a + I_d \cdot E \cdot \alpha) \quad (10)$$

and a quantity S_1' which is a quantity corresponding to the S_1 spillage factor of the donor, but determined on the double-labeled cells,

$$S_1' = (I_2/I_1)_{\text{donor + acceptor}}. \quad (11)$$

Eqs. (6) and (7) can be cast into the alternative forms:

$$r_1 = \left[(1-S \cdot S_1') \cdot r' + (S_1'-S_1) \cdot S \cdot \rho_a \cdot r_a'\right]/(1-S \cdot S_1), \quad (12)$$

$$r_2 = \left[(1-S \cdot S_1') \cdot S_1 \cdot \rho_d \cdot r' + (S_1'-S_1) \cdot r_a'\right]/\left[(1-S \cdot S_1) \cdot S_1'\right]. \quad (13)$$

From Eqs. (12) and (13) the donor and acceptor anisotropies in the presence of FRET can be expressed as:

$$r' = (r_1 - S \cdot S_1' \cdot \rho_a \cdot r_2)/(1-S \cdot S_1') \cdot (1-S \cdot S_1)/(1-S \cdot S_1 \cdot \rho_d \cdot \rho_a), \quad (14)$$

$$r_a' = (S_1' \cdot r_2 - S_1 \cdot \rho_d \cdot r_1)/(S_1'-S_1) \cdot (1-S \cdot S_1)/(1-S \cdot S_1 \cdot \rho_d \cdot \rho_a). \quad (15)$$

Based on Eqs. (14) and (15) the frequency distribution curves of the r' and r_a' anisotropies can be computed from the measured frequency distributions of the r_1, r_2, I_1, and I_2 quantities, in the knowledge of the S, S_1, ρ_d, and ρ_a spectral parameters.

In addition to the factors responsible for the spectral corrections and balancing the different channel sensitivities, the anisotropy r_a of the directly excited acceptor but on the double-labeled sample enters into the outputs of our computational algorithm (Eqs. (31)–(34)). However, since this quantity cannot be measured in the framework of the present method, its value should be estimated by the anisotropy of the single acceptor-labeled sample assuming a negligible modulation of anisotropies by a possible sterical interaction between the dye-targeting ligands. The assumption on the spatial independence of mAbs can be checked by applying an mAb pair comprised of a stained and a dim mAb.

Determination of the spectral spillage factors S, S_1 and the α factor (in Supplement) Q9 Q10

3.1.2. Case I: calculation of FRET efficiency and anisotropy of sensitized emission when the acceptor–donor intensity ratio is known

Now let's assume that, the acceptor-to-donor concentration ratio, and consequently the I_a/I_d intensity ratio – where I_a and I_d are the would-be intensity values in the absence of FRET and steric interactions – is the same constant and known value for each double-labeled cell. By designating the I_a/I_d (now constant) intensity ratio with $f_{a/d}$ i.e.

$$f_{a/d} \equiv I_a/I_d, \quad (16)$$

after taking the ratio of Eqs. (4) and (5), we obtain the following expression for the FRET efficiency:

$$E = \left[(S_1'-S_1)/(1-S \cdot S_1') - f_{a/d}\right]/\left[(S_1'-S_1)/(1-S \cdot S_1') + \alpha\right]. \quad (17)$$

By using this formula, the FRET efficiency E can be calculated for each cell, i.e. the frequency distribution of E can be determined from the

distribution of the S_1' quantity, the ratio of I_2 and I_1 measured intensity distributions. After replacing I_a/I_d with $f_{a/d}$, the acceptor anisotropy in the presence of donor (Eq. (10)) takes up the form:

$$r_a' = \left(f_{a/d} \cdot r_a + E \cdot \alpha \cdot r_{et}\right) / \left(f_{a/d} + E \cdot \alpha\right). \quad (18)$$

From Eqs. (4), (5) and (18), we can express the value of r_{et}, and I_d by using the value of E as determined by Eq. (17):

$$r_{et} = r_a' - f_{a/d} \cdot (r_a - r_a')/(E \cdot \alpha), \quad (19)$$

$$I_d = I_1/(1-E) \cdot (1-S \cdot S_1')/(1-S \cdot S_1). \quad (20)$$

Finally, by using the definition of $f_{a/d}$ (Eq. (16)) the value of I_a can be calculated as:

$$I_a = f_{a/d} \cdot I_d. \quad (21)$$

This approach can be used whenever the $f_{a/d}$ ratio can be ensured to be a predetermined known constant value for each cell. In practice this criterion can be realized in intra-molecular FRET measurements when two different epitopes of the same receptor are labeled with the donor and acceptor mAbs, or in measurements of homoassociations when the same type of mAb is used for targeting the donor and acceptor. However, also in these cases any sterical interaction between the dye-targeting ligands should be excluded to guarantee that the $f_{a/d}$ value as determined from the single-labeled samples should be valid also in the double-labeled one.

Eq. (18) may offer an in-situ alternative way for the determination of both the r_a acceptor anisotropy and the r_{et} sensitized emission anisotropy using only the FRET sample. Eq. (18) can be transformed into a linear form by isolating the fractional intensity of the sensitized emission designated by η:

$$r_a' = r_a - (r_a - r_{et}) \cdot \eta, \quad (22)$$

where η is introduced as $\eta \equiv E \cdot \alpha/(f_{a/d} + E \cdot \alpha)$. By linear fitting of the r_a' vs. η 2-dimensional correlation plots (dot-plots) according to Eq. (22), the r_a anisotropy can be obtained as the intercept (r_a = intercept) and r_{et} as the sum of the slope and the intercept. The advantage of this approach lies in that it is self-consistent, i.e. because r_a is determined in the presence of the donor mAb possible sterical effects of the donor mAb on the rotation of acceptor is automatically taken into account. A related cell-by-cell $1/r_a'$ vs. 1-E dot-plot is displayed in Fig. 1s Panel B in the Supplementary material.

3.1.3. Case II: calculation of FRET efficiency and the acceptor–donor ratio when the anisotropy of sensitized emission is known

If $f_{a/d}$ is not known, after eliminating its value from Eq. (18) by the expression

$$f_{a/d} = (S_1' - S_1) \cdot (1-E)/(1-S \cdot S_1') - E \cdot \alpha, \quad (23)$$

obtained from Eq. (17), and after isolating a parameter called t,

$$t \equiv 1/\alpha \cdot (S_1' - S_1)/(1-S \cdot S_1') \cdot (1-r_a'/r_a)/(1-r_{et}/r_a), \quad (24)$$

we arrive at the following expression for the FRET efficiency, which is now renamed as T to distinguish it from the quantity E of Case I and to refer to that the acceptor anisotropy is involved in its deduction:

$$T = t/(1+t). \quad (25)$$

The following five properties characteristic either to the method or to the FRET process itself can be read out from the formal structure of Eq. (24):

(i) *Multiplication rule:* We can see that the t quantity (~k_t, see bellow) essentially splits up to a product of two factors (notwithstanding the $1/\alpha$ scaling factor) reflecting the independence of two events. This is well in accordance with the independent operation of the two main FRET-effects: Firstly, a spectral shift of photons from the green to the red wavelength region referring to the energy dissipation during FRET is described by the first factor containing the $S_1' = I_2/I_1$ intensity ratio. Secondly, an increased orientation disordering of the excited state during FRET is characterized by the second factor containing the r_a'/r_a anisotropy ratio.

(ii) *Minimum property:* Inspecting Eqs. (24) and (25) we can see that by replacing with zero a finite positive true value of the r_{et} anisotropy of the sensitized emission we obtain a lower limit for the true value of the t parameter and the FRET efficiency T, i.e.

$$t \geq t_{min}, \quad (26)$$

and

$$T \geq T_{min}, \quad (27)$$

where the minimum value of t (t_{min}) is defined as:

$$t_{min} \equiv 1/\alpha \cdot (S_1' - S_1)/(1-SS_1') \cdot (1-r_a'/r_a), \quad (28)$$

and the minimum value of T (T_{min}) can be obtained by plugging t_{min} into Eq. (25). This "minimum property" of t indicates another power of the method: it can be safely applied also in those cases when the zero value for the r_{et} sensitized emission anisotropy is not guaranteed. By plugging the zero instead of a positive true value of r_{et} in Eq. (24) we get an under-estimation of the true energy transfer efficiency (i.e. T increases with increasing r_{et}), a step which decreases the probability of the false positive biological decisions. By comparing Eqs. (24) and (28) it can be seen that the connection between the true t value and t_{min} is $t = t_{min}/(1 - r_{et}/r_a)$. Furthermore the true t value can be computed by using the formula for t_{min}, Eq. (28), but with an α-factor corrected for the nonzero anisotropy of sensitized emission: $\alpha_{corr} = \alpha \cdot (1 - r_{et}/r_a)$..

(iii) t *is a normalized rate constant:* Additionally, by comparing Eq. (25) to the formula defining the FRET efficiency with the rate constants for FRET (k_t) and the total decay rate of the donor but in the absence of the acceptor ($1/\tau_d$, where τ_d is the donor lifetime), $E = k_t/(1/\tau_d + k_t)$, it can be deduced that:

$$t = k_t \cdot \tau_d. \quad (29)$$

Alternatively, by using Förster's formula [3,4] defining the k_t rate constant for FRET in terms of the R_0 and R distances, and the k_f fluorescence rate constant, $k_t = 1/\tau_d \cdot (R_0/R)^6$, Eq. (29) can be cast into the following form:

$$t = (R_0/R)^6. \quad (30)$$

In these formulas R_0 is the critical Förster-distance and R is the separation between a single donor and a single acceptor, or an "appropriately defined" average distance between the donor and acceptor populations.

(iv) *"All-ratio" mode:* Another remarkable feature of Eq. (24), which can be seen at a closer inspection, is that it has been built up only from ratios, i.e. it is an "all-ratio" type of an expression. As a consequence, this implies an enhanced precision in the determination of the quantities t, T and $f_{a/d}$ (compare also Eqs. (31), (32) bellow). The effect of fluctuations in the exciting light intensity and light path, due to e.g. cell wobbling in the flow cytometer, or the depth-of-field variation in microscopy will be effectively suppressed.

Please cite this article as: L. Bene, et al., Single-laser polarization FRET (polFRET) on the cell surface, Biochim. Biophys. Acta (2014), http://dx.doi.org/10.1016/j.bbamcr.2014.07.011

(v) *Independence from the donor anisotropy:*
It is interesting that the anisotropy of donor (r_1') does not appear directly in the final solution of the FRET problem (Eqs. (24), (31)–(34)), only indirectly, via the r_a' anisotropy and possibly via r_{et}. The donor anisotropy enters into the calculations merely from a technical reason: it is used only for the spectral isolation of the r_a' anisotropy from the r_2 compound anisotropy (Eq. (15)). The explicit forms of the T, $f_{a/d}$, I_d and I_a quantities can be obtained by using Eqs. (20), (21), (23)–(25) (by replacing E with T):

$$T = (S_1'-S_1)\cdot(r_a-r_a')/[\alpha\cdot(1-S\cdot S_1')\cdot(r_a-r_{et})+(S_1'-S_1)\cdot(r_a-r_a')], \quad (31)$$

$$f_{a/d} = \alpha\cdot(S_1'-S_1)\cdot(r_a'-r_{et})/[\alpha\cdot(1-S\cdot S_1')\cdot(r_a-r_{et})+(S_1'-S_1)\cdot(r_a-r_a')], \quad (32)$$

$$I_d = I_1\cdot[\alpha\cdot(1-S-S_1')\cdot(r_a-r_{et})+(S_1'-S_1)\cdot(r_a-r_a')]/[\alpha\cdot(1-S\cdot S_1)\cdot(r_a-r_{et})], \quad (33)$$

$$I_a = I_1\cdot(S_1'-S_1)/(1-S\cdot S_1')\cdot(r_a'-r_{et})/(r_a-r_{et}). \quad (34)$$

An interesting property of Eqs. (31)–(34) is that the I_a directly excited acceptor intensity does not depend on α [49], whereas the other quantities do. This follows from the fact that the I_a quantity is independent of the FRET process, whereas the others are dependent.

3.1.4. Consistency between Case I and Case II

Essentially Case I and Case II are not different, but two views of the same situation. The system of basic Eqs. (17) and (18) can be solved either for the r_{et} and E as the function of the $f_{a/d}$ intensity ratio or for the E (renamed as T for referring to the involvement of polarization) and $f_{a/d}$ quantities as the function of r_{et}, depending on whether $f_{a/d}$ or r_{et} is the known parameter. The logic behind this approach is the following: First we get an estimation of the r_{et} anisotropy of the sensitized emission for a given type of ligands (mAb or Fab of a given L labeling ratio in our case) by applying Case I for a known system of sterically non-interacting dye-targeting ligands, e.g. the L368-W6/32 mAb pair against the β_2m and heavy chain components of MHCI. Then, with the estimation of r_{et} obtained in the previous step, Case II is applied for the determination of the FRET efficiency and the $f_{a/d}$ intensity ratio for those ligand pairs when the sterical interaction cannot be excluded, e.g. in the "natural case" of homoassociation measurements when the same type of mAb is used for targeting both the donor and the acceptor, or in the case of special competing mAbs such as the L243 and W6/32 mAbs against the MHCII and MHCI receptors. Using this formalism the assumed and the true value of $f_{a/d}$ deviate just in those cases when r_{et} deviates from zero, an effective criterion for finding sterically interacting ligand pairs.

3.1.5. Modeling donor anisotropy: the associated fraction of donors

In the method the r_1 anisotropy of the donor channel is also determined, which in addition to its use for the spectral unmixing of the donor and acceptor anisotropies can also be used for the determination of the associated donor fraction (FRET-fraction) as a refinement of our cluster determination, when the rotational characteristics of the receptor-tethered fluorophore is known. The estimation of the associated donor fraction is made possible by the fact that the r_1 anisotropy of the double-labeled sample can be taken as the average over the anisotropies of the clustered and unclustered donor subpopulations (no acceptor cross-talk into the donor channel is assumed) [41]. If the associated donor fraction is denoted by f, and the unperturbed quantum efficiency of the donors by q_0 (~I_d) then the following expression can be written for r_1:

$$r_1 = [q_0\cdot f\cdot(1-T/f)\cdot r' + q_0\cdot(1-f)\cdot r]/[q_0\cdot f\cdot(1-T/f)+q_0\cdot(1-f)]. \quad (35)$$

In the first term of the numerator we have taken into account that: (i) the quantum efficiency of the clustered subpopulation of the donors is reduced by the factor 1-T/f, where T/f is the FRET efficiency in the clustered subpopulation (this is a consequence of an equation analogous to Eq. (35), but written for the quantum efficiency q of the total population which is an average over the FRET-reduced quantum efficiency of the associated donors having a transfer efficiency T_0 and the unperturbed quantum efficiency q_0 of the unclustered donors i.e. $q = q_0\cdot f\cdot(1-T_0)+q_0\cdot(1-f)$ from which $T_0 = T/f$ where $T \equiv 1-q/q_0$), (ii) the donor anisotropy in the clustered fraction r_1' is different from that in the unclustered one r, $r_1' > r$ due to FRET. In the next step we express r_1' with the detected FRET efficiency T and the associated fraction f. In the simplest approach to the anisotropy of the donor, the donor is taken as an isotropic free rotator and the validity of the Perrin-equation is assumed [41–43], i.e. the effect of any constraint is conveyed by σ through the ϕ rotational correlation time:

$$r = r_0/(1+\sigma), \quad (36)$$

where r, and r_0 designate the steady state anisotropy and the starting limiting anisotropy; the parameter σ is the ratio of the τ fluorescence lifetime and the ϕ rotational correlation time for the donor ($\sigma = \tau/\phi$), all in the absence of acceptor. If we further assume that neither the rotational correlation time nor the limiting anisotropy is altered by the acceptor, which was proved by applying unlabeled mAb with the donor labeled one, the effect of FRET can be incorporated into Eq. (36) by a (1-T/f)-fold reduction of the lifetime [14]:

$$r' = r_0/[1+\sigma\cdot(1-T/f)]. \quad (37)$$

After putting r_1' into Eq. (35), and by eliminating r_0 by using Eq. (36), the cell-by-cell distribution of f can be computed from the distributions of r_1 and T if r and σ (or equivalently r_0 and σ) are known. Eq. (35) is linear in the $T_0 = T/f$ corrected FRET efficiency for which it can be solved for:

$$T_0 = 1-\sigma'/\sigma. \quad (38)$$

Here $\sigma' = \sigma\cdot(1-T/f)$ is a rotational rate-related quantity which contains actually the anisotropy correction of the primarily measured T value:

$$\sigma' = (r_1-r)/[r/(1-T)-r_1]. \quad (39)$$

With the predetermined values of r and σ the cell-by-cell frequency distributions of σ′ and T_0 can be computed. Then the distribution of the associated fraction f can also be calculated from the distribution of T and T_0 as $f = T/T_0$:

$$f = T/(1-\sigma'/\sigma). \quad (40)$$

Since the T/f quantity should be transfer efficiency in nature, for true values of f the inequality condition

$$T/f \le 1 \quad (41)$$

Please cite this article as: L. Bene, et al., Single-laser polarization FRET (polFRET) on the cell surface, Biochim. Biophys. Acta (2014), http://dx.doi.org/10.1016/j.bbamcr.2014.07.011

should be satisfied, which translates into the following condition for the lower limit of f:

$$f \geq f_{min} = T. \quad (42)$$

According to Eqs. (41), (42) for a hypothetical 100% corrected T/f transfer efficiency, the associated fraction is minimal and equals the average transfer efficiency T. It can be proved that both the $T < T_0 < 1$ and the $f_{min} < f < 1$ inequalities are fulfilled (according to Eqs. (38), (39) from $\sigma'_\perp(r'_\perp) > \sigma'_\perp(r_1)$ follows that $T_0 > T$ because $r'_\perp > r_1$).

3.1.6. Determination of the rotational constants in the steady state

When all the donors are associated (i.e. $f = 1$ and $r_1 = r'_\perp$ e.g. in the case of the L368-W6/32 mAb pair), rotational constants can be determined in the following three ways:

(i) Based on Eq. (37), linear fitting of the $1/r'_\perp$ vs. 1-T dot-plots (consisted of the correlated 1-T, $1/r'_\perp$ value pairs of c.a. 10^4 cells) yields r_0 as the reciprocal of intercept, and the $\sigma = \tau/\phi$ as the slope/intercept ratio [14]. This method has the advantage that it is "self consistent": Because both rotational constants are determined on the same double labeled sample, the donor anisotropy in the presence of acceptor but in the absence of FRET can be obtained and by comparing it with the anisotropy of the single donor-labeled sample any influence of the acceptor mAb on the donor rotational mobility or lifetime other than FRET (steric effects) can be revealed. A minor disadvantage of this method is that because only average values of r_0 and $\sigma = \tau/\phi$ are yielded by the fitting, information about a possible cell-by-cell variation is lost.

(ii) $1/r'_\perp$ vs. 1-T Perrin-plots can also be constructed from the mean values of anisotropies and FRET efficiencies when the FRET efficiency (and the donor lifetime) is modulated by changing the labeling ratio of the acceptor mAb ensuring meantime the saturating binding condition for both the donor and acceptor mAbs [14].

(iii) When neither the rotational constants nor the lifetime of the donor are influenced by the acceptor sterically, after elimination of the $\sigma = \tau/\phi$ ratio in Eq. (37) by using Eq. (36),

$$\sigma = r_0/r - 1, \quad (43)$$

the limiting anisotropy of the donor can be expressed as a function of the measurable quantities r, $r'_\perp$ and T:

$$r_0 = r \cdot r' \cdot T/[r - r' \cdot (1 - T)]. \quad (44)$$

The importance of Eqs. (43) and (44) lies in that, with the distributions of $r'_\perp$ and T in hand, we are able to construct even the frequency distributions of the rotational parameters r_0 and $\sigma = \tau/\phi$, and the correlation of these quantities with T can be studied in dot-plots as a check for consistency of the measurement: they should be independent of T.

Theory for hindered rotations (found in the Supplementary material).

4. Experimental results

4.1. Determination of the FRET efficiency and the anisotropy of the sensitized emission: titration of the amount of acceptor

Table 1 demonstrates the feasibility of the determination of the FRET efficiency and either the anisotropy of the sensitized emission, or the unperturbed donor and acceptor intensities from the combined fluorescence anisotropy and intensity data, depending on whether the acceptor-to-donor concentration ratio or the emission anisotropy of the sensitized emission is known in advance. The light and heavy chain subunits (β_2m and h.c.) of the MHCI receptor were targeted by the donor- or acceptor-stained mAbs on the Kit-225-K6 human T-lymphoblast cells. Table 1 has been constructed by applying our basic system of equations (Eqs. (17), (18)) in two ways. (i) The first one is when energy transfer efficiency (denoted by E) is calculated from the measured S_1 and S_1' parameters assuming that the acceptor-to-donor concentration ratio $(B_a/B_d)_0$ (~$f_{a/d}$) as predetermined from the single-labeled samples is appropriate also for the double-labeled sample i.e. no sterical interaction between the dye-targeting ligands is assumed. The sense of this approach lies in the fact that in those cases when the acceptor-to-donor concentration ratio in the double-labeled sample is known (e.g. the case of sterically non-interacting ligands) the value of E can be further used for the calculation of the anisotropy of sensitized emission r_{et}. (ii) In the 2nd usage of Eqs. (17), (18) the assumption is made on the value of r_{et}, e.g. $r_{et} = 0$, and the FRET efficiency, this time denoted by T, with the unperturbed donor and acceptor intensities I_d and I_a (consequently with the acceptor-to-donor concentration ratio B_a/B_d) are calculated as functions of the r_{et} parameter (Fig. 4). More definitely, if in the 2nd approach the polarization FRET efficiency T and the unperturbed intensities I_d and I_a are computed for a true zero value of r_{et}, then these should be equal to the corresponding intensities of the single-labeled samples and the FRET efficiency E calculated according to the first approach by using the $f_{a/d}$ intensity ratio as input parameter. Furthermore r_{et} should be get back as zero. Any difference in intensity, FRET efficiency, and r_{et} implies the presence of steric interaction between the ligands.

The input parameters of the calculations for Case I are: The constants r, ρ_d, S_1, r_a, $f_{a/d}$ or $(B_a/B_d)_0$, and α determined with the single-labeled samples, and the cell-by-cell frequency distributions of r_1, r_2, S_1' determined with the double-labeled ones. The outputs of Case I are the cell-by-cell frequency distributions of E, r_{et}, I_d, I_a, and B_a/B_d. For Case II: The inputs are the constants r, ρ_d, S_1, r_a, and α determined with the single-labeled samples, the assumed $r_{et} = 0$, and the cell-by-cell frequency distributions of r_1, r_2, S_1' determined with the double-labeled ones. The outputs of Case II are the cell-by-cell frequency distributions of T, I_d, I_a, and B_a/B_d (see also Fig. 4). The values of these quantities are listed for the donor–acceptor mAb pairs L368-W6/32 (Table 1 Part A) and W6/32-W6/32 (Table 1 Part B) monitoring intramolecular FRET between the light (β_2m) and heavy chain components of the same MHCI receptor and the intermolecular FRET between the heavy chains of the MHCI governed by the degree of homoassociation of MHCI, respectively.

To reveal the effects of hetero- and homo-FRET on the measured r_1 and r_2 anisotropies, the amount of acceptor was gradually increased in the samples. Additionally, to investigate the dependence on the rotational mobility of the acceptor, the corresponding samples labeled with Fab fragments of the same antibodies (Table 1 Parts C, D) were also measured. The following general features equally valid for the four titration series could be noticed by the examination of the data:

(i) *Zero anisotropy of sensitized emission.* As expected both E and T as well as $(B_a/B_d)_0$ and B_a/B_d monotonically increase with increasing amount of acceptor for both approaches. Although, the results of the two approaches practically coincide at the larger (last three) acceptor concentrations, the values of T are systematically larger than E, and at the same time the values of B_a/B_d are systematically smaller than those of $(B_a/B_d)_0$, two related effects more pronounced for the smaller acceptor concentrations (at the first two) in all titration series. The anisotropy of the sensitized emission r_{et} follows a similar trend: although it closely approaches the value of zero at larger acceptor concentrations in all titration series, it may significantly deviate from zero in the negative direction at the smaller acceptor concentrations (Parts A–D).

(ii) *Donor and acceptor anisotropy are adversely affected by FRET.* All the donor anisotropies in the presence of acceptor (r_1) are larger

Please cite this article as: L. Bene, et al., Single-laser polarization FRET (polFRET) on the cell surface, Biochim. Biophys. Acta (2014), http://dx.doi.org/10.1016/j.bbamcr.2014.07.011

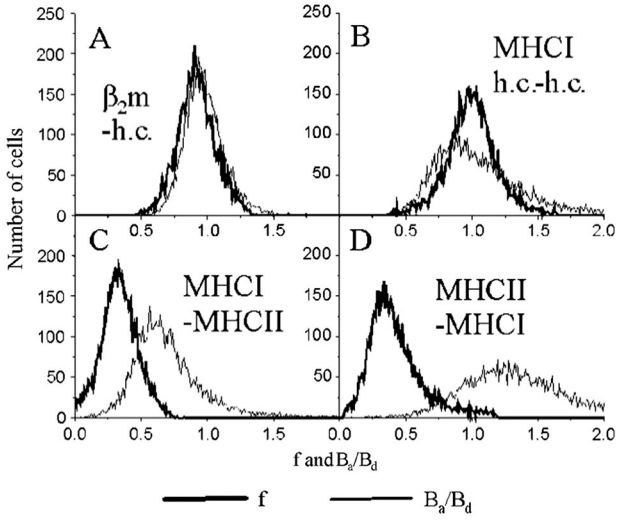

Fig. 5. Associated fraction may deviate from the acceptor-to-donor ratio. Shown are the measured frequency distributions of the associated donor fraction f (thick line) and the corresponding acceptor-to-donor concentration ratio B_a/B_d (thin line), on the surface of JY B lymphoblast cells, when the binding sites for both the donor- and acceptor-conjugated mAbs are saturated. The distribution of f was computed according to Eq. (40). Considering the distribution of B_a/B_d, first the distribution of $f_{a/d}$ was calculated according to Eq. (32), then that of B_a/B_d by using the $B_a/B_d = (\varepsilon_d/\varepsilon_a) \cdot (L_d/L_a) \cdot (f_{a/d}/\alpha)$ relationship, based on the definition of α (Eq. (1s)). Panel A: Donor-conjugated L368 mAb (anti-β_2m) and acceptor-conjugated W6/32 mAb (anti-MHCI h.c.), a donor–acceptor system monitoring intra-molecular proximity of the light chain (β_2m) and heavy chain (h.c.) subunits of the same MHCI molecule. As a consequence of the 1:1 stoichiometry of binding sites for the donor- and acceptor-conjugated mAbs, the distribution of f practically peaks at the same location as that of B_a/B_d. The frequency distribution curves of f and B_a/B_d are narrow reflecting a rather small biological variation. Panel B: both the donor and the acceptor are targeted by the W6/32 mAb to the heavy chain of the MHCI molecule, a donor–acceptor system monitoring MHCI homoassociation. In this case the frequency distribution curves are broader than those for the intra-molecular FRET. Panel C: Donor-conjugated W6/32 mAb (anti-MHCI h.c.) and acceptor-conjugated L243 mAb (anti-MHCII, DRα), a system monitoring hetero-association of the MHCI molecules with the MHCII molecules. Because in this case the number of acceptors is much smaller than the number of donors, the acceptor-to-donor ratio curve peaks substantially left to the unity. The fact that the associated fraction of the donors peaks even left to the acceptor-to-donor ratio indicates that more than one MHCII molecules should be associated with one MHCI molecule in the receptor motif. These frequency distribution curves are broader than on Panels A, B reflecting a substantial biological variation. Panel D: Donor-conjugated L243 mAb (anti-MHCII, DRα) and acceptor-conjugated W6/32 mAb (anti-MHCI h.c.), a system monitoring hetero-association of the MHCII molecules with the MHCI molecules. Because in this case the number of acceptors is much larger than the number of donors, the acceptor-to-donor ratio curve peaks substantially right to the unity – the reciprocal of that in Panel C. The fact that the associated fraction of the donors does not reach unity even in this case indicates that not all MHCII molecules are associated with the MHCI molecules, in accordance with the reversed case of Panel C, when the associated fraction did not reach the value of the acceptor-to-donor ratio. These frequency distribution curves are broad reflecting again a substantial biological variation.

than those without acceptor (r), and conversely, all the acceptor anisotropies in the presence of donor (r_2) are smaller than those in the absence of it (r_a) with differences increasing with the amount of acceptor proportionally (see also Figs. 4, 5). We can also notice that, the donor anisotropies are less affected by FRET than the acceptor anisotropies: in average 14.2 ± 2.6% increase for the donor anisotropy (r_1/r-1), and −26.2 ± 1.2% decrease for the acceptor anisotropy (r_2/r_a − 1) at the largest acceptor concentrations.

(iii) *Rotational mobility adversely modulates the sensitivity of anisotropy for the donor and the acceptor.* The anisotropy of both the acceptor-conjugated Fab fragments and whole mAbs exhibits a systematic decrease with the increasing amount of labels in each titration series. Furthermore, the donor-free anisotropy values of acceptor-labeled Fab fragments are significantly larger than those for the corresponding whole mAbs. These observations imply a dependence of sensitivity for the detection of FRET via acceptor depolarization on factors such as homo-transfer between the different acceptor-labeled antibodies (determined by the degree of homoassociation of the labeled receptor) and within each labeled ligand (determined by the dye-per-protein labeling ratio of the ligand), and the ns-time scale rotational mobility of the tethered dyes.

For comparing quantitatively the sensitivity of the anisotropies to FRET, a sensitivity parameter can be introduced as the ratio of the relative anisotropy change and the FRET efficiency: $(r_1/r-1)/T\sqrt{b^2-4ac}$ on the donor side, and $(r_2/r_a - 1)/T$ on the acceptor side. These quantities can also be conceived as the approximations to the "logarithmic derivative" of anisotropies r_1 and r_2 with respect to the FRET efficiency taken at T = 0: $d(\ln r_1)/dT|_{T=0}$ and $d(\ln r_2)/dT|_{T=0}$. Comparing the FRET-sensitivity of the acceptor anisotropy r_2 for both the acceptor-labeled Fab fragments and whole mAbs we arrive at the conclusion that the sensitivity for Fab fragments is larger than that for the whole mAbs being the sensitivity parameters −148.6 ± 23.8% and −101.7 ± 18.2%, respectively (n = 10). We remark that the sensitivity parameter can also be computed for the r_a, acceptor anisotropy, not contaminated with donor cross-talk: −165.5 ± 28.5% and −112.2 ± 20.6%, for the Fab fragment and whole mAb, respectively (n = 10). They are not much different from the corresponding sensitivities of r_2, being the donor cross-talks of r_1 relatively small. Considering the sensitivity of donor anisotropy to FRET, the analogous calculations reveal that the opposite is true: the sensitivity is larger for the whole mAb (25.6 ± 3.3%, n = 10), than for the Fab fragments (17.8 ± 2.3%, n = 5).

(iv) *Homo-transfer adversely modulates sensitivity of anisotropy for the donor and the acceptor.* With a similar calculation applied to the first and last samples of the titration series it can be shown that by increasing the amount of acceptor the sensitivity of acceptor anisotropy is reduced from −209.9 ± 32.2% to −67.8 ± 12.8% (n = 4) by homo-FRET. Interestingly enough, the sensitivity of the r_1 donor anisotropy was increased proportionally with the amount of acceptor from 20.5 ± 7.3% to 40.7 ± 11.4% (n = 4).

Reference measurements with rFLIM reinforce the zero anisotropy for sensitized emission (found in the Supplementary material). Q11

4.2. FRET between MHCI and MHCII

Table 2 lists anisotropy, FRET efficiency and acceptor-to-donor concentration ratio data for FRET measured between antibodies against the MHCI and MHCII antigens on Kit-225-K6 human T-lymphoblast cells. The FRET samples have been titrated according to the amount of the acceptor mAb for each FRET pair (as above between epitopes of MHCI) and data belonging to the largest (saturating) acceptor concentrations are listed. To reveal a possible effect of the rotational mobility of the acceptor on the resolution in detecting FRET, the samples have been constructed with both whole mAbs and Fab fragments being the rotational mobility of the latter more constrained than that of the former [57–62]. Because the anisotropy of the sensitized emission r_{et} was calculated according to the conventional method (Eq. (19)) by using the FRET efficiency values E (Eq. (18)), we expect that any deviation in r_{et} from zero reports on systematic errors in the assumed acceptor-to-donor ratios.

Inspecting the values of r_{et} the following general trends can be noticed regardless whether Fab fragments or whole mAbs were used: (i) Many r_{et} values deviate from zero in the negative direction with only a few exceptions. (ii) For samples monitoring intramolecular FRET on the MHCI molecule or the homoassociation of MHCI, the deviations are not significant: −0.024 ± 0.020, n = 8. (iii) The statistically significant deviations of r_{et} belong to samples monitoring heteroassociations of MHCI with MHCII: −0.174 ± 0.050, n = 6. We

Table 2
FRET efficiencies and fluorescence anisotropies measured for different donor–acceptor pairs on the surface of Kit-225-K6 T-lymphoma cells.

Donor (AF488-conjugated)		Acceptor (AF546-conjugated)		Single-labeled samples		Double-labeled samples						
mAb	Antigen	mAb	Antigen	r	r_a	r_1	r_2	E (%)[a]	r_{et}	$(B_a/B_d)_0$[b]	T (%)[a]	B_a/B_d[b]
Part A, whole mAbs												
L368	β_2m	L368	β_2m	0.216 ± 0.009[c]	0.210 ± 0.023	0.244 ± 0.002	0.173 ± 0.015	18.6 ± 5.7	−0.025 ± 0.073	0.398 ± 0.055	20.8 ± 3.4	0.355 ± 0.039
		W632	MHCI h.c.		0.193 ± 0.013	0.252 ± 0.009	0.159 ± 0.008	41.2 ± 7.4	−0.072 ± 0.053	1.024 ± 0.024	45.1 ± 4.2	0.935 ± 0.057
		L243	MHCII		0.191 ± 0.002	0.236 ± 0.005	0.173 ± 0.001	27.7 ± 1.9	−0.068 ± 0.050	0.739 ± 0.030	30.9 ± 0.6	0.662 ± 0.054
Part B, whole mAbs												
W6/32	MHCI h.c.	L368	β_2m	0.190 ± 0.007	0.210 ± 0.023	0.228 ± 0.003	0.137 ± 0.014	31.9 ± 2.3	−0.035 ± 0.027	0.799 ± 0.037	35.1 ± 1.4	0.727 ± 0.066
		W632	MHCI h.c.		0.187 ± 0.034	0.227 ± 0.008	0.137 ± 0.021	44.5 ± 2.0	0.027 ± 0.003	0.738 ± 0.028	42.3 ± 3.3	0.776 ± 0.033
		L243	MHCII		0.191 ± 0.002	0.213 ± 0.004	0.134 ± 0.009	23.8 ± 4.6	−0.114 ± 0.094	0.756 ± 0.030	31.3 ± 1.4	0.574 ± 0.098
Part C, whole mAbs												
L243	MHCII	W632	MHCI h.c.	0.213 ± 0.008	0.186 ± 0.002	0.232 ± 0.008	0.152 ± 0.002	25.1 ± 6.3	−0.244 ± 0.098	1.355 ± 0.041	35.0 ± 2.0	0.970 ± 0.018
Part D, Fab fragments												
L368 Fab	β_2m	L368 Fab	β_2m	0.230 ± 0.007	0.271 ± 0.012	0.242 ± 0.002	0.212 ± 0.002	8.9 ± 2.8	−0.081 ± 0.004	0.434 ± 0.105	13.4 ± 1.4	0.395 ± 0.101
		W6/32 Fab	MHCI h.c.		0.256 ± 0.011	0.262 ± 0.007	0.173 ± 0.003	25.6 ± 11.1	0.018 ± 0.042	0.947 ± 0.028	34.4 ± 4.5	0.784 ± 0.176
		L243 Fab	MHCII		0.237 ± 0.004	0.244 ± 0.003	0.169 ± 0.002	12.1 ± 1.3	−0.323 ± 0.060	0.713 ± 0.038	17.1 ± 0.9	0.503 ± 0.019
Part E, Fab fragments												
W6/32 Fab	MHCI h.c.	L368 Fab	β_2m	0.210 ± 0.007	0.267 ± 0.019	0.226 ± 0.002	0.165 ± 0.002	18.0 ± 0.7	−0.026 ± 0.002	1.010 ± 0.244	19.5 ± 1.4	0.926 ± 0.177
		W6/32 Fab	MHCI h.c.		0.247 ± 0.011	0.249 ± 0.005	0.162 ± 0.003	41.9 ± 7.3	0.062 ± 0.027	0.246 ± 0.015	27.0 ± 3.5	0.382 ± 0.080
		L243 Fab	MHCII		0.237 ± 0.004	0.229 ± 0.002	0.187 ± 0.002	22.9 ± 2.2	0.050 ± 0.021	0.495 ± 0.037	17.6 ± 0.7	0.644 ± 0.049
Part F, Fab fragments												
L243 Fab	MHCII	W6/32 Fab	MHCI h.c.	0.230 ± 0.002	0.270 ± 0.005	0.247 ± 0.002	0.205 ± 0.015	16.3 ± 0.9	−0.271 ± 0.032	1.451 ± 0.100	20.9 ± 1.5	1.129 ± 0.113

[a] FRET efficiencies computed without and with fluorescence anisotropy are designated by E and T, respectively. Determination of E is based on acceptor–donor receptor number ratios $(B_a/B_d)_0$ obtained from single-labeled samples.
[b] Acceptor–donor receptor number ratios determined from single- and double-labeled samples are designated by $(B_a/B_d)_0$ and B_a/B_d, respectively.
[c] Values are averages and their standard deviations (SEM) obtained from 5 independent measurements. These values belong to the highest acceptor concentrations in titration series similar to those shown in Table 1.

also notice that, the deviation of the polarization FRET efficiency T from the conventional FRET efficiency E follows a similar trend: 12.8 ± 8.6%, n = 8 for the MHCI homoassociation and the intramolecular FRET and 57.3 ± 17.9%, n = 6 for the MHCI–MHCII heteroassociation. The corresponding deviations of the acceptor-to-donor concentration ratio B_a/B_d from $(B_a/B_d)_0$ are: −8.7 ± 4.7%, n = 8 and −19.8 ± 4.1%, n = 6. If the results of the polarization FRET method is accepted to be true based on the assumption that $r_{et} = 0$, from these findings we can see that just in those cases when r_{et} is significantly smaller than zero, i.e. the cases of the MHCI–MHCII heteroassociation, the FRET efficiency is underestimated and the acceptor-to-donor ratio is overestimated by the conventional method. According to the theory behind the two approaches, this finding implies a significant sterical interaction between the corresponding L243 and W6/32 mAbs targeting the MHCII and MHCI receptors, respectively.

As to the acceptor anisotropies r_a and r_2, the significantly larger values (30.6 ± 2.8% and 20.3 ± 5.4%, respectively, n = 7) found for the Fab fragments as compared to the whole mAbs implies a larger dynamic range for decreasing anisotropy due to energy transfer and consequently a larger precision manifested in smaller width of e.g. transfer efficiency and $f_{a/d}$ histograms and ultimately in a larger resolution of FRET detection through polarized intensities.

As a more quantitative evaluation of the sensitivity of anisotropies to FRET, by comparing the index of sensitivity – introduced in the previous section as the relative change in anisotropy per unit FRET efficiency – for Fab fragments and whole mAbs we can see that while at the acceptor side the sensitivity for Fab fragments is definitely larger than for whole mAbs (−125.1 ± 19.4% and −72.5 ± 13.6%, respectively, n = 7), at the donor side just the opposite is true: the sensitivity for the Fab fragments is smaller than for the whole mAbs (27.8 ± 6.6% and 44.4 ± 8.9%, respectively, n = 7). Interestingly, the magnitudes of sensitivity parameters for the acceptor anisotropy are much larger than those for the donor anisotropy. By comparing the ratios of the sensitivity parameters, the general conclusion can be drawn that acceptor anisotropy is much more sensitive to changes in FRET than donor anisotropy.

Hindered rotation of mAbs, experimental (found in the Supplementary material).

Q12

4.3. Determination of associated fractions

Cell-by-cell distribution of acceptor-to-donor concentration ratios (B_a/B_d), corrected energy transfer efficiencies (T/f), and associated donor fractions (f) were computed according to Eqs. (32), (38), (40) by using the rotational constants of Table 2 s (Fig. 5). The importance of these quantities lies in that they make possible a refined analysis of the structure of receptor clusters e.g. via comparing f to B_a/B_d (Fig. 6, see also in Section 5).

The mean values of the B_a/B_d, f, $T = f_{min}$ and T/f histograms as well as the deduced n_d/n_a stoichiometric ratio (Eq. (45)) of the receptor motifs are listed for the Kit-225-K6 and JY cells in Table 5 for the homo- and hetero-associations of the MHCI and MHCII receptors. The associated fractions between the light and heavy chains of the MHCI molecule (Table 5, Panel A of Figs. 5, 6) have been found 100% in both cell lines showing the consistency between the fitting procedure for obtaining the rotational constants and the cell-by-cell computation of the associated fractions. Furthermore, on both cell lines near 100% associated fractions have been found for the MHCI homoassociation (Table 3, Panel B of Figs. 5, 6). In these cases the corrected FRET efficiencies practically coincide with the primarily measured uncorrected ones.

5. Discussion

5.1. Polarization FRET (polFRET) algorithms

In this work a novel method for the detection of FRET has been worked out based on the simultaneous detection of the anisotropy of the donor and acceptor in addition to the conventional FRET indicators such as the quenched donor intensity and the sensitized emission of the acceptor (Figs. 1, 4). The method is based on the condition that the anisotropy of the sensitized emission is zero [15,17,21]. Due to its importance, the nill condition of sensitized emission anisotropy were examined and found to be valid for our random FRET systems realized by the donor- and acceptor-conjugated mAbs bound to the cell surface. After the spectral demixing of the fluorescence anisotropies and intensities measured in the donor and acceptor channels by adding the acceptor anisotropy as an extra parameter to the conventionally detected donor and acceptor intensities we arrive at a system of three equations (Eqs. (16)–(18)) which can be applied in two ways.

Case I: For FRET systems using sterically noninteracting labels the acceptor-to-donor intensity ratio can be determined from the single-labeled samples and the system of equations can be solved for the three unknowns, the E FRET efficiency (designated by E to remind that it is a function of the assumed acceptor-to-donor intensity ratio in this case), the r_{et} anisotropy of the sensitized emission, and the I_d unquenched donor intensity.

Case II: With an assumed value (e.g. nill) of the r_{et} anisotropy of sensitized emission as a free parameter, the number of equations is just enough for the complete description of an energy transfer system i.e.

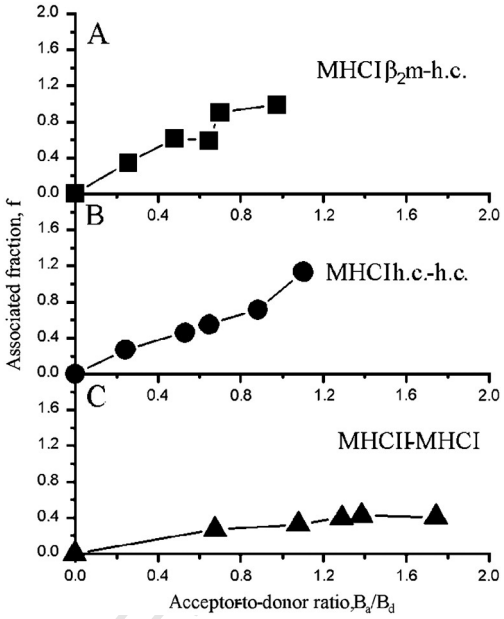

Fig. 6. The fine structure of receptor clusters can be described by the associated fraction-acceptor-to-donor ratio curves. Lateral distribution of receptors determines the form of dependence of associated fraction on the acceptor-to-donor concentration ratio on the surface of Kit-225-K6 T-lymphoblast cells. In the panels associated fraction of the donors (f) is plotted as the function of acceptor-to-donor concentration ratio (B_a/B_d). The plotted values are means of histograms like those shown in Fig. 6. Panel A: FRET between the donor-labeled L368 mAb (anti-β_2m) and the acceptor-labeled W6/32 mAb (anti-MHCI h.c.), a donor–acceptor system monitoring intra-molecular proximity of the light chain (β_2m) and heavy chain (h.c.) subunits of the same MHCI molecule. As a consequence of the 1:1 stoichiometry of binding sites for the donor- and acceptor-conjugated mAbs, the associated fraction linearly increases with the acceptor-to-donor ratio and saturates at unity at the unit acceptor-to-donor ratio. The linearity of this dependence proves also the consistency between the determination of the rotational constants and the computation of the associated fraction. Panel B: FRET when both donor and acceptor are targeted by the W6/32 mAb to the heavy chain of the MHCI molecule, a donor–acceptor system monitoring MHCI homoassociation. The associated fraction approximately linearly increases with the acceptor-to-donor ratio but in contrast to the case of the MHCI intramolecular FRET, it does not saturate at unit acceptor-to-donor ratio. Panel C: FRET between donor-labeled L243 mAb (anti-MHCII, DRα) and acceptor-labeled W6/32 mAb (anti-MHCI h.c.), a system monitoring hetero-association of the MHCII and MHCI molecules. This curve deviates from those in Panels A and B in two ways: (i) It saturates already at small acceptor-to-donor ratios. (ii) The saturating value of the associated fraction is much smaller than unity.

Please cite this article as: L. Bene, et al., Single-laser polarization FRET (polFRET) on the cell surface, Biochim. Biophys. Acta (2014), http://dx.doi.org/10.1016/j.bbamcr.2014.07.011

Table 3
Associated donor fractions and acceptor-to-donor concentration ratios measured on Kit-225-K6 T- and JY B-lymphoma cells.

Donor (AF488-conjugated)		Acceptor (AF546-conjugated)		Acceptor-to-donor ratio	Associated fractions		Stoichiometric ratio	Energy transfer efficiency	
					Donor	Acceptor		Uncorrected	Corrected
mAb[a]	Antigen	mAb[a]	Antigen	B_a/B_d[b]	f (%)[b]	f_a (%)[b]	n_d/n_a[c]	$T = f_{min}$ (%)	T/f (%)[d]
Part A, Kit-225-K6 cells									
L368	β_2m	W6/32	MHCI h.c.	1.203 ± 0.062[e]	98.2 ± 5.1	89.2 ± 13.4	0.915 ± 0.153	38.5 ± 3.4	39.2 ± 4.0
W6/32	MHCI h.c.	L368	β_2m	0.727 ± 0.062	89.2 ± 13.4	98.2 ± 5.1	1.249 ± 0.225	25.1 ± 0.9	28.1 ± 4.3
L368 Fab	β_2m	W6/32 Fab	MHCI h.c.	1.074 ± 0.161	71.8 ± 16.5	92.6 ± 11.3	0.722 ± 0.216	27.2 ± 0.9	47.9 ± 12.6
W6/32 Fab	MHCI h.c.	L368 Fab	β_2m	0.926 ± 0.113	96.0 ± 12.8	71.8 ± 16.5	1.444 ± 0.422	18.8 ± 1.5	19.6 ± 3.0
W6/32	MHCI h.c.	W6/32	MHCI h.c.	0.859 ± 0.083	95.9 ± 11.9	100	1.116 ± 0.176	37.0 ± 2.9	38.6 ± 5.7
W6/32		L243	MHCII, DRα	0.434 ± 0.015	49.8 ± 2.9	42.1 ± 2.2	2.726 ± 0.233	33.1 ± 1.6	66.5 ± 5.0
L368	β_2m	L243		0.662 ± 0.054	47.9 ± 7.7	42.1 ± 2.2	1.719 ± 0.323	30.6 ± 2.0	63.9 ± 11.1
L243	MHCII, DRα	W6/32	MHCI h.c.	0.970 ± 0.015	47.1 ± 4.1	48.9 ± 4.1	0.994 ± 0.121	29.3 ± 1.1	62.2 ± 5.9
L243 Fab		W6/32 Fab		1.129 ± 0.048	37.1 ± 1.5	48.9 ± 4.1	0.673 ± 0.093	24.2 ± 1.0	65.2 ± 3.7
Part B, JY cells									
L368 Fab	β_2m	W6/32	MHCI h.c.	0.838 ± 0.140	94.5 ± 4.1	84.8 ± 9.5	1.330 ± 0.274	44.5 ± 2.4	47.1 ± 3.3
L368 Fab		W6/32 Fab		0.887 ± 0.059	82.0 ± 14.9	84.8 ± 9.5	1.090 ± 0.244	35.9 ± 1.4	43.8 ± 8.1
W6/32	MHCI h.c.	W6/32	MHCI h.c.	0.785 ± 0.129	85.5 ± 9.4	100	1.089 ± 0.215	32.7 ± 4.9	38.2 ± 7.1
W6/32		L243	MHCII, DRα	0.848 ± 0.095	28.4 ± 4.3	69.9 ± 4.7	0.479 ± 0.096	9.7 ± 2.3	34.2 ± 9.6
L243	MHCII, DRα	W6/32	MHCI h.c.	1.279 ± 0.186	90.5 ± 8.6	28.4 ± 4.3	2.491 ± 0.574	59.7 ± 0.5	65.9 ± 6.3
L243 Fab		W6/32		0.852 ± 0.059	51.9 ± 2.1	28.4 ± 4.3	2.145 ± 0.367	45.9 ± 1.8	88.4 ± 4.9
L243 Fab		W6/32 Fab		1.089 ± 0.051	67.5 ± 11.1	28.4 ± 4.3	2.184 ± 0.498	40.1 ± 0.5	59.4 ± 9.8

[a] The labeling ratios varied in the ranges 1.86–2.77 and 0.89–1.57 for the whole mAbs and Fabs, respectively.
[b] Acceptor-to-donor concentration ratio is defined as the ratio of the number of receptors actually occupied by the acceptor- and donor-conjugated mAbs in the double-labeled sample, as determined with the polFRET formalism (Case II). It can be calculated from the measured donor and acceptor intensities I_d and I_a unperturbed by FRET (Eq. (32)) by taking into account the different detectibility and absorptions of the donor and acceptor dyes, as well as the different labeling ratios of the dye-targeting mAbs: $B_a/B_d = (1/\alpha) \cdot (\varepsilon_d/\varepsilon_a) \cdot (L_d/L_a) \cdot (I_a/I_d)$, where ε_d and ε_a are the molar decadic absorption coefficients of the dyes, L_d and L_a are the labeling ratios of the donor- and acceptor-conjugated mAbs. The α factor corrects for the different detectibilities of the donor and acceptor dyes in the two detection channels. The values of f were computed according to Eq. (40). The value of f_a is just the average of the f values of the reverse donor–acceptor pairs. For the transfer pairs monitoring homoassociations the f_a is assumed to be 100% when $B_a/B_d < 1$.
[c] The n_d/n_a stoichiometric ratio was calculated based on Eq. (45).
[d] Because the corrected energy transfer efficiency should be smaller than unity, the associated fraction should be larger than the uncorrected energy transfer efficiency: $f > T = f_{min}$.
[e] Values are averages and their standard deviations (SEM) obtained from 5 independent measurements. These values belong to the highest acceptor concentrations in titration series similar to those displayed in Table 1.

for the determination of the T FRET efficiency (called "polarization FRET efficiency" and designated by T to remind us that it is a function of r_{et} in this case), and the unperturbed (by FRET) donor and acceptor intensities I_d and I_a, two signals which are proportional to the donor and acceptor concentrations in the double-labeled sample (Eqs. (31)–(34), Fig. 4). For the r_{et} anisotropy of the sensitized emission, zero was used, partly based on the theory of randomly oriented donor–acceptor systems, partly on our observation that it can practically be taken as nill for the donor and acceptor dyes tethered to the surface bound mAbs. An interesting feature of this procedure is that, although the r_1 donor anisotropy is also detected, it does not appear directly in the final solution for the three unknowns (Eqs. (31)–(34)). It is used only in the spectral isolation of the acceptor anisotropy (Eq. (15)).

Comparison of the polarization FRET (polFRET) algorithms with the dual laser FRET (FCET) justifies the zero value of the sensitized emission anisotropy (found in the Supplementary material).

5.2. The associated fraction (f) is characteristic to the morphology of receptor patterns

The computation of the FRET efficiency and the two quantities proportional to the amount of donor and acceptor is based on the total intensity of the donor and acceptor, as well as the anisotropy of acceptor. Because the anisotropy of the donor does not play a direct role in the determination of these quantities, it is not involved in the formulas of the final solution of the problem, i.e. in Eqs. (31)–(34). However, it does play an indirect role, it is needed for "cleaning" of the signals: for unmixing of the donor and acceptor anisotropies (Eqs. (14), (15)).

The donor anisotropy gains explicit usage in the determination of a quantity characteristic to the structure of receptor clusters, the associated fraction of the donor (Table 3). The simultaneous detection of the FRET efficiency and the donor anisotropy makes possible the determination of the associated fraction in the knowledge of the rotational constants (r_0, $\sigma = \tau/\phi$ and r_∞) of the donor (Figs. 5, 6). The latter quantities can be determined e.g. by fitting the reciprocal anisotropy vs. 1-T dot-plots with suitable rotational models for samples where the associated fraction is 100% (Table 2 s, Fig. 1s Panel A). In addition to that the associated fraction can be regarded as an indicator of the lifetime heterogeneity of the donor population, by examining the dependence of associated fraction on the acceptor-to-donor occupied receptor ratio we can obtain valuable information on the structure of the supporting receptor clusters [7,10,21,50–52].

The relationship between the associated fractions and the structure of receptor patterns can be envisioned e.g. by using a quasi-random model of receptor associations [10,21]. In the framework of this model the receptor clusters are conceived as repetitions of some kind of an association unit or receptor motif comprised of a central receptor and at most six (in average) peripheral ones. This type of a cluster model is corroborated by two facts: (i) The receptors behave as incompressible hard cores. (ii) FRET is essentially confined to the first neighbors, being the diameter of a typical receptor very close to the Förster critical distance (5.6 nm). The concept of receptor motifs makes possible the representation of receptor clusters by only 6 numbers: the total number of binding sites for the donor- and acceptor-conjugated ligands (B_d, B_a), the average number of donor- and acceptor-bearing receptors in a receptor motif (n_d, n_a) – dictated by local stoichiometry –, and the associated fractions of the binding sites for the donor- and acceptor-conjugated ligands (f, f_a). The explicit dependence of the associated fraction of the donors on the acceptor-to-donor ratio is described by the following equation:

$$f = f_a \cdot B_a/B_d \cdot n_d/n_a, \quad (45)$$

which can be obtained by solving for f the "balance equation" $f \cdot B_d/n_d = f_a \cdot B_a/n_a$ expressing "conservation" of receptor numbers.

To visualize the dependence of the f associated fraction of donors on the B_a/B_d acceptor-to-donor concentration ratio we analyze three special cases based on Eq. (45). We assume that the donor bearing receptors are saturated in all cases. (i) In the case of a 1:1 association of receptors, i.e. when $n_d = n_a$ (e.g. two subunits of a molecule, the light and heavy chain of the MHCI), the associated fraction closely follows the acceptor-to-donor (receptor) ratio at the different acceptor levels (Fig. 6 Panels A, B). (ii) If several acceptor-bearing receptors are associated with a donor-bearing receptor, i.e. when $n_d < n_a$ (e.g. heteroassociation between two receptors of different expression levels, association of MHCII bearing donor with MHCI bearing acceptor), then the associated fraction of donors is smaller than the acceptor-to-donor ratio (Fig. 6 Panel C). (iii) If the associated fraction of donors is larger than the acceptor-to-donor ratio, i.e. when $f > B_a/B_d$, then several donor-bearing receptors are associated with an acceptor-bearing receptor, i.e. then $n_d > n_a$. Interestingly, from the inverse condition $n_d > n_a$ does not follow unambiguously that $f > B_a/B_d$, and similarly the inverse condition $f < B_a/B_d$ cannot be translated unambiguously to $n_d < n_a$ due to the condition $f_a < 1$. The essence of this paragraph can be summed up in the following rule: any deviation from the 1:1 association stoichiometry translates into a corresponding deviation (either up or down) of the associated fraction vs. acceptor-to-donor ratio curve from the direct proportionality curve, i.e. the 45°-angle straight line with high probability.

The data in Table 3 were calculated in the spirit of the above receptor motif model and by using Eq. (45) for the calculation of the stoichiometric ratios (n_d/n_a). In spite of the similar expression levels, and as a consequence similar acceptor-to-donor (B_a/B_d) ratios, we have found striking differences in the associating properties of the MHCI and MHCII molecules on the investigated cell lines. By designating the MHCI as the "donor receptor" and MHCII as the "acceptor receptor" we have found the average n_d/n_a stoichiometric ratio to be 1.734 ± 0.362 and 0.451 ± 0.094 on the Kit-225-K6 cells and JY cells, respectively. The associated fractions of the MHCI and MHCII molecules in the heteroassociations on the Kit-225-K6 cells are $48.9 \pm 4.1\%$ and $42.1 \pm 5.0\%$ (with $B_a/B_d = 75.3 \pm 13.0\%$), respectively (Fig. 6 Panel C). On the JY cells they are $28.4 \pm 4.3\%$ and $69.9 \pm 11.2\%$ (with $B_a/B_d = 93.0 \pm 8.6\%$) (Fig. 5 Panels C, D).

The essence of these structural data can be summarized in the following models of receptor clustering: While on Kit-225-K6 cells roughly half of the MHCI and MHCII molecules take part in the formation of the MHCI–MHCII receptor motifs at a ~2:1 stoichiometric ratio, on the JY cells only one-third of the MHCI molecules associate with two-third of the MHCII molecules with a ~1:2 stoichiometry. In other words, the heteroassociations on Kit-225-K6 cells comprise mainly of MHCI, on JY cells mainly of MHCII molecules. This observation well corresponds to the function of these cell lines played in the antigen presentation, namely that the Kit-225-K6 cells – a T cell line – present the foreign antigen mainly by the MHCI molecules, and the JY cells – a B cell line – mainly by the MHCII molecules. The detected associated fractions are in good agreement with our earlier cluster determinations with atomic force microscopy [31], cross-correlation confocal microscopy [32], as well as homo-FRET analysis [21].

5.3. Sensitivity of the polarization FRET method: factors affecting resolution

First, the general principles behind the response of donor and acceptor anisotropies in sensing FRET are discussed, then our results are evaluated according to these principles. Based on the fact that donor anisotropy should be increased and acceptor anisotropy should be decreased by energy transfer, the main factors determining the sensitivity of anisotropies are merely the steady state anisotropy values of the donor and acceptor: r and r_a assuming finite positive values of r_0. On the donor side, smaller values of r favor detection of FRET, being the dynamic range $r_0 - r$ larger. The opposite is true at the acceptor side: here larger r_a values favor detection of FRET, being the dynamic range simply the value of r_a. Because donor anisotropy plays no direct role in the determination of FRET efficiency in the present method the only prerequisite for the applicability of the method is a high enough value of acceptor anisotropy r_a.

5.4. Criteria for the applicability of fluorophores

As to the mere detectibility of FRET, the method is applicable inasmuch as FRET leads to noticeable acceptor depolarization independently of the value of the donor anisotropy r_1, due to the fact that FRET efficiency as determined with polarization (Eqs. (24), (31)) does not depend on the donor anisotropy. Donor anisotropy is needed only for spectral isolation of the acceptor anisotropy in the presence of donor r_a' according to Eq. (15). In respect of FRET detectibility, the requirement of a high dynamic range may give a hint on the physical nature of acceptor fluorophores which can be used. Dipole emitters of high r_0 limiting anisotropy with static random orientations like engineered visible fluorescent proteins (VFPs) whose rotational Brownian motion is largely impaired by the β-barrel cage [51–53], and dyes impregnated in highly viscous solvents e.g. plastics, glasses are amongst the best acceptors. In contrast, dipole emitters with large degree of rotational freedom, like dyes dissolved in low viscosity solvents, and near-isotropic (multipole, quadrupole or higher order) emitters, like certain quantum dots (QDs), fluorophores with degenerate transitions, and atomic emitters, like Europium, Therbium (lanthanides) are amongst the worst acceptors, due to their small r_0 value [24,52–56,63,65]. However, on the donor side, as to the further application of the method for the determination of the associated donor fraction f, the applicability of donor anisotropy r_1 for computation of associated fraction f rests on the presence and abundance of FRET sensitive rotational modes, i.e. rotational rates comparable to the rate constant for FRET [14]. Fluorescent dyes the rotational dynamics of which are either severely hindered (high r) at the one end, or very intensive (low r_0) at the other end, or having electronic transitions of symmetry higher than dipole's (e.g. "mixed polarizations") are amongst the worst donors in sensing FRET via anisotropy [14,63]. The best donors are those whose rotational rates are close to the rate of FRET – a kind of "resonance condition". The method can also be advantageously used in the case of ligand-tethered dyes, like in our case, which have highly constrained rotational motion manifested in rather high r_a values. In this respect the Fab fragments are better dye-carriers than the whole mAbs, as the rotational motion of Fabs is more hindered than that of the whole mAbs, the latter possessing a substantial hinge motion [57–62].

5.5. Implications for averaging regime and distribution of the orientation factor for FRET (κ^2)

Summarizing the aforementioned in terms of averaging regimes for the orientation factor κ^2, while the mere detection of FRET seems to require acceptors falling into the isotropic static averaging regime, the averaging regime of donors can be arbitrary. However, for the determination of associated donor fraction, donors falling into the intermediate averaging regime are needed [18–20,22]. As to our Alexa dyes targeted to the receptors via tethering to the whole mAb and Fab systems as the linkers (L243 anti-MHCII, L368 and W6/32 anti-MHCI), they fall into the intermediate averaging regime as revealed by the sensitivity of the donor anisotropy r_1 to FRET (Fig. 1s Panel A) [14]. This implies that distributions of κ^2 with means falling between 0.475 – for isotropic static orientations – and 0.67 – for isotropic dynamic orientations – can be hypothesized in these cases [18–20,22].

We saw how the orientation distributions encoded in the donor and acceptor anisotropies may help measure FRET efficiency T via Eqs. (24), (31). However, another dependence of FRET efficiency T on the orientation distributions of the donor and acceptor orientations enters via Eq. (30), where the appropriate R_0 characteristic Förster-distance should be defined by the mean of the aforementioned – and as yet

experimentally not known – κ^2 distribution obeying intermediate averaging regime: $R_0 = (3 \cdot \kappa^2/2)^{1/6} \cdot R_{0,2/3}$, where $R_{0,2/3}$ means the characteristic Förster-distance belonging to isotropic dynamic averaging, i.e. $\kappa^2 = 2/3$. However, the independent averaging of κ^2 and donor–acceptor separation (R) leading to Eq. (30) can be done only approximately, when FRET and orientations are not independent. Mutual dependence of FRET and orientations in our case arises for the reason that molecular reorientations and FRET take place on the same time-scale ("intermediate averaging") [71]. Relative orientations and FRET would be uncoupled if the fluorophores would perform complete reorientations during the excited state lifetime or the transitions involved in FRET would be isotopically degenerate, implying also $\kappa^2 = 2/3$, and zero anisotropy for both the donor and acceptor. However this is not the case in our situation, because at least the acceptor anisotropy should be higher than zero for the applicability of the method.

Detailed knowledge of the κ^2 distribution is not available at this time. However for near-zero values of κ^2 FRET would not be possible, whereas high values of κ^2 would not contribute to changes in polarization. It is reasonable to assume, therefore, that the κ^2 distribution, which may depend on the FRET efficiency, has a narrow peak around an intermediate value, so that the effective value of κ^2 in the R_0 of Eq. (30) may be replaced by this intermediate value. The special case of a delta-peak around $\kappa^2 = 2/3$ is not realistic, because such a distribution could only be consistent with zero values of the anisotropy for both donor and acceptor [71].

5.6. Fulfillment of the criteria for mAb-tethered dyes

We now turn to interpreting our results in the framework of the above general principles. Although both donor and acceptor anisotropies are significantly modulated by FRET, it is clear from Fig. 4 Panels A, B and Fig. 1s, that the acceptor anisotropy responds more readily to FRET than donor anisotropy for our donor–acceptor systems. The origin of this difference lies in the fact that while the donor anisotropy can increase from a rather large initial value of r (~0.22) up to reaching the limiting anisotropy r_0 (~0.32), the acceptor anisotropy drops from a rather large initial value r_a (~0.24) to essentially zero, i.e. the r_0–r dynamic range for the donor anisotropy (~0.1) is smaller than (c.a. half of) that for the acceptor anisotropy, which is equal to r_a. We should add that also the presence of an unassociated portion of the donors can be interpreted as a condition reducing sensitivity of donor anisotropy to FRET.

For optimizing the experimental conditions for achieving maximal sensitivities, we examined how the dynamic ranges are affected by the experimental conditions such as the rotational mobility of the dye-targeting mAbs and the degree of homo-FRET between dyes on the same mAb, due to a large labeling ratio or between the fluorescently labeled receptors, due to their possible homoassociation [14,21]. By comparing the Fab fragments with the whole versions of the mAbs we can see that while the dynamic range (r_0–r) for the donor anisotropy did not change significantly (~0.13 vs. ~0.1), that for the acceptor anisotropy significantly increased (~0.26 vs. ~0.19) when Fab fragments were used instead of whole mAbs. This difference is explained by the somewhat higher starting anisotropies of the Fab fragments compared to those for the whole mAbs due to the (i) the smaller rotational mobility of the Fab fragments – no hinge motion of the single Fab fragment – (ii) absence of homo-transfer on the Fab fragment, being its labeling ratio around 1. In contrast to the Fab fragments, in the whole mAbs the hinge-motion of the free (not bound to receptor) Fab and Fc arms and the larger dye-per protein labeling ratio (can be larger than 2) may reduce the anisotropy. We should add that the sensitivity of acceptor anisotropy can also be enhanced for some degree by increasing the excitation wavelength, because the anisotropy is generally higher at the long wavelength portion of the absorption spectrum, at the red edge, where homo-FRET is severely impaired (Weber-effect), albeit at the cost of reduced fluorescence intensity [64,65]. For the donor, reducing excitation wavelength would increase sensitivity, for the same reasons.

5.7. Distribution width of FRET efficiency

Sensitivity has also consequences concerning the widths of cell-by-cell frequency distribution curves of the different quantities (t, T, f, T/f, B_a/B_d). By the application of the error propagation formalism presented in the Supplementary material, our earlier statement that the sensitivity of acceptor anisotropy is determined by its starting value can also be supported quantitatively. The coefficient of variation CV_t of the cell-by-cell frequency distribution for e.g. the FRET related quantity t (Eq. 15 s) reduces implying higher sensitivity with increasing values of the r_a starting acceptor anisotropy. For its proof, it should be proved first that the 3rd (covariance) term is positive. By assuming equal polarized intensity CVs, i.e. $CV^2_{I_{2vh}} = CV^2_{I_{2vv}}$, it can be seen that the sign of the 3rd term in Eq. (15 s) is governed by the value of r_2: it is positive whenever $r_2 < 0.5 \cdot [a(\psi) - 1]/a(\psi) = 0.21$, which is satisfied because in almost all of the cases $r_2 < 0.187$ (see the values of r_2 in Tables 1, 2). Now, by increasing r_a in the denominator of the 2nd and 3rd positive terms, CV_t decreases.

"r_a′ does not decrease monotonously with increasing acceptor concentration" and "Lifetime heterogeneity decreases detected anisotropy" (in the Supplementary material).

5.8. Ratio detection and the lack of "polarization bias"

We are stressing the high accuracy and precision of our measuring technique: the high accuracy stems from the simultaneous detection of the donor quenching and sensitized emission, the high level of precision lies in that all uncertainties due to the instabilities in the power of light source and in the light path drop out since most of the calculations are based on signal ratios (see Eqs. (15), (1s), (32), (33)). A remarkable feature in our approach is that, by the pure nature of the polarization detection scheme, it is free of the so called "polarization bias" [42,70], a systematic error introduced by the lack of detection of the 3rd polarized signal component (as is the case e.g. in many flow cytometers in their basic configurations). At an observation direction orthogonal to the traveling direction of the illuminating light beam, the detected signal is proportional to $I_{vv} + I_{vh}$ instead of $I_{vv} + 2 \cdot I_{vh}$, leading to a systematic error in the measured FRET efficiency – known also from direct lifetime measurements [23] –, whose magnitude and sign depends on the anisotropy of the sample, and the polarization direction of the exciting light. In addition to the separate detection of the vertically and horizontally polarized components, this effect can be eliminated also by either exciting or detecting under the "magic angle" polarization direction [42,43,66]. It refers to either detecting unpolarized intensity excited at 54.7° from the vertical, or detecting polarized intensity at 54.7° relative to the polarization direction of the exciting light, which can be either vertical or horizontal. This phenomenon can show not only its wrong facet but also a good one: it can be exploited advantageously for ultrasensitive detection of fluorescence anisotropy in a different measuring scheme, when the sample is excited by a light beam of alternating polarization direction produced by a photoelastic modulator (PEM) [67].

5.9. Earlier works on polarization FRET and associated fraction

Interpretation of the measured FRET data can be substantially refined if we take into account the orientation properties of FRET manifested in the characteristic modulation of fluorescence anisotropy of the donor and acceptor as suggested by T.M. Jovin and R.E. Dale in their pioneering papers in the late seventies [22,43]. In the field of fluorescence microscopy recently Rizzo et al. [68] drew attention on the acceptor anisotropy as a potential new contrast parameter.

Also in fluorescence microscopy, Mattheyses et al. [69] worked out recently a related method based on the acceptor polarization for FRET analysis. In principle, this method well parallels with the dual wavelength flow cytometric FRET method (FCET) [6,11], in that the 3 unknowns of the FRET problem – the concentration of donor and acceptor, and of the FRET-pair, which is equivalent to the knowledge of FRET-efficiency – are obtained by detecting the donor intensity and two acceptor intensities excited at the donor and acceptor absorption maxima. Although this method works well with spatially separated light beams – as in the cytometer – but the simultaneous excitation required for fast imaging was ensured by the authors at the cost of changing the polarization direction of one of the exciting light beams, the acceptor's – "polarization imprinting" as they call it – and detecting the two orthogonally polarized components of the acceptor emission in addition to the unpolarized donor intensity. Although this method does not require a presumption on the value of the sensitized emission anisotropy r_{et} – notwithstanding the only minor limitation that the fluorescence polarization of the FRET-pair should be different from that of the acceptor –, as in our present case, its use is seriously limited by the need for a special sample saturated with FRET-pairs in addition to the single donor- and acceptor-labeled samples for the calculation of the nine "equipment factors". Additionally, information on the rotational dynamics remains buried in the "equipment factors", since the donor and acceptor anisotropies are not determined explicitly in their computational algorithm.

Esposito et al. [7] used a completely different principle for discriminating the clustered and unclustered donor fractions: in the frequency domain (or phase-modulation) scheme of lifetime detection the difference between the modulation lifetime and the phase lifetime is an indicator of the lifetime heterogeneity – i.e. the heterogeneity in FRET because FRET efficiency (E) can be translated into lifetime through the $E = 1 - \tau_{da}/\tau_d$ relationship where τ_d, τ_{da} are the donor lifetimes in the absence and presence of acceptor, respectively. Our approach for the determination of the associated donor fraction is similar to this in that the role of the modulation lifetime and phase lifetime is taken over by the FRET-modulated (r') and the unmodulated (r) donor anisotropies, respectively.

5.10. Conclusion and perspectives

A new method is presented for the simultaneous cell-by-cell measurement of the donor and acceptor anisotropy as well as the FRET efficiency and the acceptor-to-donor concentration ratio. The application of the method makes possible a more detailed description of the structure and dynamics of cell surface receptor patterns through the combined measurement of rotational mobility and proximity. By the combined measurement of donor anisotropy and FRET efficiency, associated fraction of donors can be determined whose functional dependence on the acceptor-to-donor concentration ratio is characteristic to the structure of the receptor cluster. Although the method is presented by focusing on a flow cytometer using a single laser excitation it can also be readily applied in a fluorescence microscope. In fluorescence imaging microscopy the role of the individual cells is taken over by the pixels, otherwise the same formalism can be used.

Considering further possibilities awaiting for elaboration, the method can be developed in several directions: (i) Based on the principle that the donor and acceptor anisotropies are simultaneously detected with the FRET efficiency, the method can be readily extended in a direction of a "Dale-Eisinger style" analysis – the simultaneous analysis of donor and acceptor anisotropies and FRET – [4,18–20,22] when the contributions of the orientation factor for FRET (κ^2) and distance in an observed change in FRET efficiency can be separated, an approach which would have much importance also in the field of single molecule fluorescence due to the lack of averaging out the effects of the orientation factor [70]. Because the donor and acceptor anisotropies are both detected in addition to FRET, our method enables the estimation of the distribution of orientation factor for FRET (κ^2), and as a consequence, the deduction of distance distributions from the FRET efficiency distributions [18–20]. Such a determination of distance distributions is not straightforward, however, as the κ^2-induced distance distribution must be distinguished from other causes of a spread in distances as a result of lateral diffusion, for example. (ii) In the present work first the total intensities and anisotropies were determined from the polarized intensity components, then from the total intensities and anisotropies the FRET efficiencies and the other quantities were deduced. However, this sequence of steps can be reversed: akin to way of determination of FRET efficiencies from the total intensities, four new FRET efficiency-like quantities can be computed also directly from the polarized intensity components of the donor and acceptor, which can be called the "polarized components of FRET efficiency" or "polarized FRET indexes". This can also be envisioned as a kind of splitting the FRET efficiency into polarized components, just like the lifetime does [23]. Because these four quantities are direct functions of the FRET efficiency and anisotropies some of them might have enhanced sensitivity for detecting subtle conformational changes. These quantities can also be conceived as "generalized FRET efficiencies", since – after G. Weber's parametric theory of rotational depolarization [72] – the rotation of the excited state might be interpreted as a special kind of FRET process between two orientations. (iii) The polarized version of the dual laser flow cytometric FRET method (FCET) can also be elaborated. Here, in addition to the donor and acceptor anisotropies excited at the absorption maximum of the donor, the anisotropy of acceptor excited at its absorption maximum is also detected. The advantages offered by the dual laser method as compared to the present, single laser version are that the anisotropy of sensitized emission r_{et} can be obtained simultaneously with the FRET efficiency, and the r_a acceptor anisotropy unperturbed by the donor can also be determined real time on the double-labeled cells. Possible sterical interactions between the donor- and acceptor-targeting labels (mAbs) can be revealed by comparing r_a and the $r_{2,a}$ anisotropy of the single acceptor labeled sample. (iv) Fast dual-polarization imaging using the presented algorithm could be realized by applying a four-way (quadrant) image splitter. (v) Concerning potential "anisotropy fluorescence lifetime imaging microscopy" (rFLIM) applications, the detection of the polarized phase angles and modulation factors in addition to the intensities could lend new opportunities for a further refinement of the characterization of receptor clusters [7,13].

Error propagation: coefficient of variation for the FRET efficiency, the acceptor-to-donor intensity ratio, the associated donor fraction, "The lower limit for the detectable FRET efficiency", "The polarization bias of FRET efficiency" (found in the Supplementary material).

6. Uncited references

[45,46,47,48]

Acknowledgments

Financial support for this work was provided by TÁMOP-4.2.2.A-11/1/KONV-2012-0045 project co-financed by the European Union and the European Social Fund, and OTKA Bridging Fund support OSTRAT/810/213 by the University of Debrecen. The authors are indebted to Dr. T.M. Jovin for making possible rFLIM measurements in the framework of a short term EMBO fellowship, ASTF no. 201-06, to the Max Planck Institute for Biophysical Chemistry, Department of Molecular Biology, Göttingen to L.B. The authors thank one of the Reviewers for the helpful comments on κ^2. Thanks are due to Prof. J. Szöllősi for his critical reading of the manuscript. Thanks are due to Ms. R. Szabó for her skilful assistance in cell culturing and sample preparations. Thanks are due to Dr. M. Bagdány, for helpful discussions on FRET and his help in surveying FRET applications.

Appendix A. Supplementary data

Supplementary data to this article can be found online at http://dx.doi.org/10.1016/j.bbamcr.2014.07.011.

References

[1] B.W. van der Meer, Ch. 3 Förster theory, in: I. Medinzt, N. Hildebrandt (Eds.), FRET—Förster resonance energy transfer: from theory to applications, 1th edition Wiley-VCH, 2013.
[2] E.A. Jares-Erijman, T.M. Jovin, FRET imaging, Nat. Biotechnol. 21 (11) (2003) 1387–1395.
[3] J.R. Lakowicz, Energy transfer. Ch. 13, Principles of Fluorescence Spectroscopy, Kluwer Academic/Plenum Publishers, New York, 1999, pp. 368–391.
[4] R.M. Clegg, Förster resonance energy transfer-FRET what is it, why do it, and how it's done. Ch. 1, in: FRET and FLIM techniques. Laboratory techniques in biochemistry and molecular biology. Vol. 33. TWJ Gadella ed., S Pillai, PC van der Vliet series eds. Elsevier, 2009 pp. 1–48
[5] A. Periasami, R.N. Day (Eds.), Molecular Imaging: FRET Microscopy and Spectroscopy, 1th edition Academic Press, 2011, pp. 1–307.
[6] L. Trón, J. Szöllősi, S. Damjanovich, S.H. Helliwell, D.J. Arndt-Jovin, T.M. Jovin, Flow cytometric measurements of fluorescence resonance energy transfer on cell surfaces. Quantitative evaluation of the transfer efficiency on a cell-by-cell basis, Biophys. J. 45 (1984) 939–946.
[7] A. Esposito, H.C. Gerritsen, F.S. Wouters, Fluorescence lifetime heterogeneity resolution in the frequency domain by lifetime moments analysis, Biophys. J. 89 (2005) 4286–4299.
[8] Z. Bacsó, L. Bene, A. Bodnár, J. Matkó, S. Damjanovich, A photobleaching energy transfer analysis of CD8/MHC-I and LFA-1/ICAM-1 interactions in CTL-target cell conjugates, Immunol. Lett. 54 (1996) 151–156.
[9] R.M. Young, J.K. Arnette, D.A. Roess, B.G. Barisas, Quantitation of fluorescence energy transfer between cell surface proteins via fluorescence donor photobleaching kinetics, Biophys. J. 67 (1994) 881–888.
[10] H. Wallrabe, M. Elangovan, A. Burchard, A. Periasamy, M. Barroso, Confocal FRET Microscopy to measure clustering of ligand-receptor complexes in endocytic membranes, Biophys. J. 85 (2003) 559–571.
[11] L. Trón, Experimental methods to measure fluorescence resonance energy transfer, in: S. Damjanovich, J. Szöllősi, L. Trón, M. Edidin (Eds.), Mobility and proximity in biological membranes, CRC Press, Boca Raton, FL, 1994, pp. 1–47.
[12] Z. Lakos, Á. Szarka, L. Koszorús, B. Somogyi, Quenching-resolved emission anisotropy: a steady state fluorescence method to study protein dynamics, J. Photochem. Photobiol. B 27 (1995) 55–60.
[13] A.H.A. Clayton, Q.S. Hanley, D.J. Arndt-Jovin, V. Subramaniam, T.M. Jovin, Dynamic fluorescence anisotropy imaging microscopy in the frequency domain (rFLIM), Biophys. J. 83 (2002) 1631–1649.
[14] L. Bene, M.J. Fulwyler, S. Damjanovich, Detection of receptor clustering by flow cytometric fluorescence anisotropy measurements, Cytometry 40 (2000) 292–306.
[15] A. Jabłoński, On the emission anisotropy of fluorescence emitted by acceptor molecules dissimilar to donor molecules in isotropic solutions, Bulletin de L'Academie Polonaise des Sciences, Série des sciences math., astr. et phys., XIX(2), 1971, pp. 171–174.
[16] S.S. Chan, D.J. Arndt-Jovin, T.M. Jovin, Proximity of lectin receptors on the cell surface measured by fluorescence energy transfer in a flow system, J. Histochem. Cytochem. 27 (1) (1978) 56–64.
[17] M.N. Berberan-Santos, B. Valeur, Fluorescence depolarization by electronic energy transfer in donor–acceptor pairs of like and unlike chromophores, J. Chem. Phys. 95 (1991) 8048–8055.
[18] B.W. van der Meer, Orientational aspects in pair energy transfer, in: D.L. Andrews, A. A. Demidov (Eds.), Resonance energy transfer, J. Wiley & Sons, New York, 1999, pp. 151–172.
[19] B.W. van der Meer, Kappa-squared: from nuisance to new sense, Rev. Mol. Biotechnol. 82 (2002) 181–196.
[20] B.W. van der Meer, Optimizing the orientation factor KAPPA-SQUARED for more accurate FRET measurements. Ch. 4 in FRET—Förster resonance energy transfer: from theory to applications, in: I. Medinzt, N. Hildebrandt (Eds.), 1th edition Wiley-VCH, 2013.
[21] L. Bene, J. Szöllősi, G. Szentesi, L. Damjanovich, R. Gáspár Jr., T.A. Waldmann, S. Damjanovich, Detection of receptor trimers on the cell surface by flow cytometric fluorescence energy homotransfer measurements, Biochim. Biophys. Acta, Mol. Cell. Res. 1744 (2005) 176–198.
[22] R.E. Dale, J. Eisinger, W.E. Blumberg, The orientational freedom of molecular probes. The orientation factor in intramolecular energy transfer, Biophys. J. 26 (1979) 161–194.
[23] R.D. Spencer, G. Weber, Influence of Brownian rotations and energy transfer upon the measurements of fluorescence lifetime, J. Chem. Phys. 52 (4) (1970) 1654–1663.
[24] D.S. Lidke, P. Nagy, B.G. Barisas, R. Heintzmann, J.N. Post, K.A. Lidke, A.H. Clayton, D.J. Arndt-Jovin, T.M. Jovin, Imaging molecular interactions in cells by dynamic and static fluorescence anisotropy (rFLIM and emFRET), Biochem. Soc. Trans. 31 (2003) 1020–1027.
[25] J. Szöllősi, L. Mátyus, L. Trón, M. Balázs, I. Ember, M.J. Fulwyler, S. Damjanovich, Flow cytometric measurements of fluorescence energy transfer using single laser excitation, Cytometry 8 (1987) 120–128.
[26] L. Bene, M. Balázs, J. Matkó, J. Möst, M.P. Dierich, J. Szöllősi, S. Damjanovich, Lateral organization of the ICAM-1 molecule at the surface of human lymphoblasts: a possible model for its co-distribution with the IL-2 receptor, class I and class II HLA molecules, Eur. J. Immunol. 24 (1994) 2115–2123.
[27] J. Szöllősi, S. Damjanovich, M. Balázs, P. Nagy, L. Trón, M.J. Fulwyler, F.M. Brodsky, Physical association between MHC class I and class II molecules detected on the cell surface by flow cytometric energy transfer, J. Immunol. 143 (1989) 208–213.
[28] J. Szöllősi, V. Hořejší, L. Bene, P. Angelisová, S. Damjanovich, Supramolecular complexes of MHC class I, MHC class II, CD20, and Tetraspan molecules (CD53, CD81, and CD82) at the surface of a B cell line JY, J. Immunol. 157 (1996) 2939–2946.
[29] S. Damjanovich, L. Bene, J. Matkó, A. Alileche, C.K. Goldman, S. Sharrow, T.A. Waldmann, Preassembly of interleukin 2 (IL-2) receptor subunits on resting Kit 225 K6 T cells and their modulation by IL-2, IL-7, and IL-15: A fluorescence resonance energy transfer study, Proc. Natl. Acad. Sci. U. S. A. 94 (1997) 3134–13139.
[30] S. Damjanovich, L. Bene, J. Matkó, L. Mátyus, Z. Krasznai, G. Szabó Jr., C. Pieri, R. Gáspár Jr., J. Szöllősi, Two-dimensional receptor patterns in the plasma membrane of cells. A critical evaluation of their identification, origin and information content, Biophys. Chem. 82 (1999) 99–108.
[31] A. Jenei, S. Varga, L. Bene, L. Mátyus, A. Bodnár, Z. Bacsó, C. Pieri, R. Jr, T. Farkas Gáspár, S. Damjanovich, HLA class I and II antigens are partially co clustered in the plasma membrane of human lymphoblastoid cells, Proc. Natl. Acad. Sci. U. S. A. 94 (1997) 7269–7274.
[32] G. Vereb, J. Matkó, G. Vámosi, S.M. Ibrahim, E. Magyar, S. Varga, J. Szöllősi, A. Jenei, R. Waldmann Jr., T.A. Gáspár, S. Damjanovich, Cholesterol-dependent clustering of IL-2Rα and its colocalization with HLA and CD48 on T lymphoma cells suggest their functional association with lipid rafts, Proc. Natl. Acad. Sci. U. S. A. 97 (11) (2000) 6013–6018.
[33] T. Hori, T. Uchiyama, M. Tsudo, H. Umadome, H. Ohno, S. Fukuhara, K. Kita, H. Uchino, Establishment of an interleukin 2-dependent human T cell line from a patient with T cell chronic lymphocytic leukemia who is not infected with human T cell leukemia/lymphoma virus, Blood 70 (1987) 1069–1073.
[34] F.M. Terhorst, P. Parham, D.L. Mann, J.L. Strominger, Structure of HLA antigens: amino-acid and carbohydrate compositions and NH_2-terminal sequences of four antigen preparations, Proc. Natl. Acad. Sci. U. S. A. 73 (1976) 910–914.
[35] C.J. Barnstable, W.F. Bodmer, G. Brown, G. Galfré, C. Milstein, A.F. Williams, A. Ziegler, Production of monoclonal antibodies to group A erythrocytes, HLA and other human cell surface anigens—new tools for genetic analysis, Cell 14 (1978) 9–20.
[36] M. Tanabe, M. Sekimata, S. Ferrone, M. Takiguchi, Structural and functional analysis of monomorphic determinants recognized by monoclonal antibodies reacting with HLA class I alpha 3 domain, J. Immunol. 148 (1992) 3202–3209.
[37] M. Edidin, T. Wei, Lateral diffusion of H-2 antigens on mouse fibroblasts, J. Cell Biol. 95 (1982) 458–462.
[38] J. Matkó, M. Edidin, Energy transfer methods for detecting molecular clusters on cell surfaces, Methods Enzymol. 278 (1997) 444–462.
[39] E.G. Spack Jr., B. Packard, M.L. Wier, M. Edidin, Hydrophobic adsorption chromatography to reduce nonspecific staining by rhodamine-labeled antibodies, Anal. Biochem. 158 (1986) 233–237.
[40] S. De Petris, Immunoelectron microscopy and immunofluorescence in membrane biology, in: E.D. Korn (Ed.), Methods in Membrane Biology, vol. 9, Plenum Press, New York, 1978, pp. 1–201.
[41] J.R. Lakowicz, Fluorescence anisotropy. Ch. 10, Principles of Fluorescence Spectroscopy, Kluwer Academic/Plenum Publishers, New York, 1999, pp. 291–318.
[42] B. Valeur, Fluorescence polarization. Emission anisotropy, Molecular fluorescence. Principles and applications, Wiley-VCH, Weinheim, 2002, pp. 125–154.
[43] T.M. Jovin, Fluorescence polarization and energy transfer: theory and application, in: M. Melamed, P. Mullaney, M. Mendelsohn (Eds.), Flow Cytometry and Sorting, J. Wiley & Sons, New York, 1979, pp. 137–165.
[44] G. Szentesi, G. Horváth, I. Bori, G. Vámosi, J. Szöllősi, R. Gáspár, S. Damjanovich, A. Jenei, L. Mátyus, Computer program for determining fluorescence energy transfer efficiency from flow cytometric data on a cell-by-cell basis, Comput. Methods Prog. Biomed. 75 (2004) 201–211.
[45] J. Siegel, K. Suhling, S. Lévêque-Fort, S.E.D. Webb, D.M. Davis, D. Phillips, Y. Sabharwal, P.M.W. French, Wide-field time-resolved fluorescence anisotropy imaging (TR-FAIM): imaging the rotational mobility of a fluorophore, Rev. Sci. Instrum. 74 (1) (2003) 182–192.
[46] C.L. Luengo Hendriks, B. Rieger, M. van Ginkel, G.M.P. van Kempen, L.J. van Vliet, DIPimage: a scientific image processing toolbox for MATLAB, Delft Univ. Technol., Delft, The Netherlands, 1999. (Online available: http://www.qi.tnw.tudelft.nl/DIPlib).
[47] P. Nagy, G. Vámosi, A. Bodnár, S.J. Lockett, J. Szöllősi, Intensity-based energy transfer measurements in digital imaging microscopy, Eur. Biophys. J. 27 (1998) 377–389.
[48] P. Nagy, L. Bene, W.C. Hyun, G. Vereb, M. Braun, C. Antz, J. Paysan, S. Damjanovich, J.W. Park, J. Szöllősi, Novel calibration method for flow cytometric fluorescence resonance energy transfer measurements between visible fluorescent proteins, Cytometry A 67A (2005) 86–96.
[49] L. Bene, T. Ungvári, R. Fedor, László Sasi-Szabó, L. Damjanovich, Intensity correlation-based calibration of FRET, Biophys. J. 105 (2013) 1–13.
[50] T.G. Dewey, M.M. Datta, Determination of the fractal dimension of membrane protein aggregates using fluorescence energy transfer, Biophys. J. 56 (1989) 415–420.
[51] A.K. Kenworthy, M. Edidin, Distribution of a glycosylphosphatidylinositol-anchored protein at the apical surface of MDCK cells examined at a resolution of <100 Å using imaging fluorescence resonance energy transfer, J. Cell Biol. 142 (1) (1998) 69–84.
[52] D.A. Zacharias, J.D. Violin, A.C. Newton, R.Y. Tsien, Partitioning of lipid-modified monomeric GFPs into membrane microdomains of live cells, Science 296 (2002) 913–916.
[53] A. Volkmer, V. Subramaniam, D.J.S. Birch, T.M. Jovin, One- and two-photon excited fluorescence lifetimes and anisotropy decays of green fluorescent proteins, Biophys. J. 78 (2000) 1589–1598.

Please cite this article as: L. Bene, et al., Single-laser polarization FRET (polFRET) on the cell surface, Biochim. Biophys. Acta (2014), http://dx.doi.org/10.1016/j.bbamcr.2014.07.011

[54] I. Gautier, M. Tramier, C. Durieux, J. Coppey, R.B. Pansu, J.-C. Nicolas, K. Kemnitz, M. Coppey-Moisan, Homo-FRET microscopy in living cells to measure monomer–dimer transition of GFP-tagged proteins, Biophys. J. 80 (2001) 3000–3008.
[55] J.V. Rocheleau, M. Edidin, D.W. Piston, Intrasequence GFP in class I MHC molecules, a rigid probe for fluorescence anisotropy measurements of the membrane environment, Biophys. J. 84 (2003) 4078–4086.
[56] S.V. Gaponenko, Absorption and emission of light by semiconductor nanocrystals. Ch. 5, in: P.L. Knight, A. Miller (Eds.), Optical properties of semiconductor nanocrystals. Cambridge studies in modern optics, Cambridge University Press, Cambridge, 1989, pp. 84–151.
[57] D.C. Hanson, J. Yguerabide, V.N. Schumaker, Segmental flexibility of immunoglobulin G antibody molecules in solution: a new interpretation, Biochemistry 20 (1981) 6842–6852.
[58] V.T. Oi, T.M. Vuong, R. Hardy, J. Reidler, J. Dangl, L.A. Herzenberg, L. Stryer, Correlation between segmental flexibility and effector function of antibodies, Nature 307 (1984) 136–140.
[59] W.P. Schneider, T.G. Wensel, L. Stryer, V.T. Oi, Genetically engineered immunoglobulins reveal structural features controlling segmental flexibility, Proc. Natl. Acad. Sci. U. S. A. 85 (1988) 2509–2513.
[60] J.L. Dangl, T.G. Wensel, S.L. Morrison, L. Stryer, L.A. Herzenberg, V.T. Oi, Segmental flexibility and complement fixation of genetically engineered chimeric human, rabbit and mouse antibodies, EMBO J. 7 (7) (1988) 1989–1994.
[61] O.H. Brekke, T.E. Michaelsen, I. Sandlie, The structural requirements for complement activation by IgG: does it hinge on the hinge? Immunol. Today 6 (2) (1995) 85–90.
[62] B. Carrasco, J. Garcia de la Torre, O. Byron, D. King, C. Walters, S. Jones, S.E. Harding, Novel size-independent modeling of the dilute solution conformation of the immunoglobulin IgG Fab′ domain using SOLPRO and ELLIPS, Biophys. J. 77 (1999) 2902–2910.
[63] E. Haas, E. Katchalski-Katzir, I.Z. Steinberg, Effect of orientation of donor and acceptor on the probability of energy transfer involving electronic transitions of mixed polarization, Biochemistry 17 (23) (1978) 5064–5070.
[64] G. Weber, M. Shinitzky, Failure of energy transfer between identical aromatic molecules on excitation at the long wave edge of the absorption spectrum, Proc. Natl. Acad. Sci. U. S. A. 65 (4) (1970) 823–830.
[65] A. Squire, P.J. Verveer, O. Rocks, P.I.H. Bastiens, Red-edge anisotropy microscopy enables dynamic imaging of homo-FRET between green fluorescent proteins in cells, J. Struct. Biol. 147 (2004) 62–69.
[66] C.L. Asbury, J.L. Uy, G. van den Engh, Polarization of scatter and fluorescence signals in flow cytometry, Cytometry 40 (2000) 88–101.
[67] D. Canet, K. Doering, C.M. Dobson, Y. Dupont, High-sensitivity fluorescence anisotropy detection of protein-folding events: application to α-Lactalbumin, Biophys. J. 80 (2001) 1996–2003.
[68] M.A. Rizzo, D.W. Piston, High-contrast imaging of fluorescent protein FRET by fluorescence polarization microscopy, Eur. Biophys. J. Biophys. Lett. (2005), http://dx.doi.org/10.1529/biophysj.104.055442.
[69] A.L. Mattheyses, A.D. Hoppe, D. Axelrod, Polarized fluorescence resonance energy transfer microscopy, Biophys. J. 87 (2004) 2787–2797.
[70] L. Cognet, G.S. Harms, G.A. Blab, P.H.M. Lommerse, T. Schmidt, Simultaneous dual-color and dual-polarization imaging of single molecules, Appl. Phys. Lett. 77 (24) (2000) 4052–4054.
[71] B.W. van der Meer, M.A. Raymer, S.L. Wagoner, R.L. Hackney, J.M. Beechem, E. Gratton, Designing matrix models for fluorescence energy transfer between moving donors and acceptors, Biophys. J. 64 (1993) 1243–1263.
[72] G. Weber, Perrin revisited: parametric theory of the motional depolarization of fluorescence, J. Phys. Chem. 93 (1989) 6069–6073.

Please cite this article as: L. Bene, et al., Single-laser polarization FRET (polFRET) on the cell surface, Biochim. Biophys. Acta (2014), http://dx.doi.org/10.1016/j.bbamcr.2014.07.011